Article:
Krishnaraj, C, Jena, HS, Leus, K et al. (3 more authors) (2019) An aliphatic hexene-covalent triazine framework for selective acetylene/methane and ethylene/methane separation. Journal of Materials Chemistry A, 7 (21). pp. 13188-13196. ISSN 2050-7488

https://doi.org/10.1039/c8ta11722e

An aliphatic Hexene-Covalent Triazine Framework for Selective Acetylene/Methane and Ethylene/Methane Separation

Chidharth Krishnaraj[1], Himanshu Sekhar Jena[1], Karen Leus[1], Helen M. Freeman[2], Liane G. Benning[2,3,4], Pascal Van Der Voort[1]*

[1] COMOC, Center for Ordered Materials, Organometallics and Catalysis, Department of Chemistry, Ghent University, 9000 – Gent, Belgium

[2] GFZ, German Research Center for Geosciences, Telegrafenberg, 14473 Potsdam, Germany

[3] Department of Earth Sciences, Free University of Berlin, 12249 Berlin, Germany

[4] School of Earth and Environment, University of Leeds, Leeds LS2 9JT, United Kingdom

Abstract:

Unsaturated C_2 hydrocarbons (acetylene and ethylene) are used in industries for various applications. These C_2 hydrocarbons are produced through cracking processes, where, C_1 hydrocarbons such as methane are usually present as a by-product. The conventional distillation process for C_2/C_1 hydrocarbon separation uses a lot of energy and as such microporous adsorbents are widely studied as low energy alternatives. Herein, we present a novel hexene-covalent triazine framework (Hexene-CTF) prepared from trans-3-Hexenedinitrile (an aliphatic olefin type monomer) for high-performance acetylene/methane and ethylene/methane separation. The porosity, surface area and ordering of the materials were varied by changing the synthesis conditions. The characteristics of the material were characterized thoroughly by surface area analysis as well as transmission and scanning electron microscopy (TEM and SEM) measurements. The number of double bonds present within the CTF materials was determined by a bromine addition reaction. A high uptake of acetylene (3.85 mmol/g at 0°C and 1 bar) was obtained. The presence of unsaturated double bonds in the Hexene-CTF enhanced the interaction of the framework with the unsaturated double bond and triple bond of ethylene and acetylene respectively due to stronger pi-pi interactions. On the contrary, the saturated methane gas was not efficiently adsorbed, which resulted in a higher C_2/C_1 selectivity. The calculated isosteric heat of adsorption showed a direct correlation between the gas uptake and the ordering in the Hexene-CTF at low pressure regimes. This is the first example of a porous organic polymer which is capable of C_2/C_1 hydrocarbon separation.

Introduction

C_2 hydrocarbons such as acetylene (C_2H_2) and ethylene (C_2H_4) are important raw materials in the petrochemical industries.[1] C_2H_2 gas is used worldwide for several applications including portable blowtorch[2], processing polymeric films[3] and synthesis of Vitamin A.[4] It is produced by cracking of petroleum[5,6] and generally contains methane (CH_4) as a C_1 hydrocarbon by-product.[5,6] C_2H_4 is another important raw material for several consumer products such as polyethylene, ethylene oxide, ethylene dichloride and ethylbenzene[7]. It is produced through industrial scale steam cracking of gaseous (ethane, propane, or butane) or liquid feedstocks (naphtha), where larger

hydrocarbons are broken to smaller ones and unsaturation is introduced.[8,9] However, several side products such as methane, propene, raw pyrolysis gasoline (RPG), hydrogen and buta-1,3-diene are also produced. Particularly, with propane or a naphtha feedstock, a 2:3 or 1:2 ratio of methane:ethylene is produced respectively.[8,9] Conventionally a cryogenic distillation method is used for such small C_2/C_1 hydrocarbon separation which is based on the difference in boiling points or vapor pressures.[10,11] Consequently, these processes consume a lot of energy and there is a constant search to develop new methods for olefin/paraffin separation.[12] Alternatively, microporous adsorbents[13] which can (i) selectively separate acetylene and ethylene from methane at room temperature and, (ii) are energy and cost-effective can be used.

Several microporous adsorbents have been used for such C_2/C_1 separation. In particular, Metal-Organic Frameworks (MOFs) have been studied for acetylene/methane separation. MOFs contain metal ions or metal clusters that are connected with each other by rigid organic linkers to form an extended framework.[14] Among the MOF based adsorbents, the FJ1-H8 material has been reported to exhibit the highest gravimetric acetylene uptake of 9.46 mmol/g at 22°C and 1 atm.[15] Cu-TDPAT also shows high acetylene uptake of 7.5 mmol/g at 22°C and 1 atm with a good selectivity over CH_4 (127.1).[16] Additionally, ZJU-198a material was reported to have a very high C_2H_2/CH_4 selectivity of 497.9 and 391.1 at 0°C and 25°C respectively.[17] However, for the latter material, in comparison to other MOFs, the acetylene uptake was rather moderate (~3.78 mmol/g at 296 K and 1 atm). In the case of ethylene/methane separation, an adsorption-hydration method was employed by Zhang *et al.* (2015) in a wet ZIF-8 material as a strategy to separate C_2H_4/CH_4 gas mixtures where the highest selectivity obtained was 5.56.[18] More recently, a ZIF-67/water-ethylene glycol slurry was used by Pan *et al.* (2016) to recover C_2H_4 from C_2H_4/CH_4 mixtures.[19] The selectivity coefficients at 10°C for ethylene glycol, water and solid ZIF-67 were 3.7, 4.7 and 3.1 respectively. This was increased to 6.3 using ZIF-67/water-ethylene glycol slurry through the absorption-adsorption hybrid method, yet the selectivity coefficient at room temperature was only 3.6. In general MOFs display high gas uptakes and selectivities due to the presence of the metal in the framework, which exhibits a strong interaction with the adsorbed gas molecules.[20,21] However, the upscaling of such functionalized MOFs is expensive as it depends on specially functionalized or complex organic and metallic components. MOFs also require toxic chemicals like dimethyl formamide (DMF) for synthesis.[22,23] In addition, most well-known MOFs tend to be sensitive to atmospheric conditions.[24] As gas separation applications often occur under harsh conditions (for example: flue gas separation)[25] usage of specialized MOFs is not preferred due to stability problems.

Recently, Covalent Organic Frameworks (COFs) have been used for various gas adsorption and storage applications.[26,27] These light-weight alternative materials follow reticular construction principles that allow prediction of the structure beforehand. This enables tunable pore size and functionalities of the porous materials with strong covalent bonds that keep the materials both mechanically and chemically stable. Among COFs, particularly, Covalent Triazine Frameworks (CTFs) are widely studied materials for applications in gas adsorption and storage, catalysis and chromatography.[28] In general, they are prepared through an ionothermal synthesis route using

the trimerization of dinitrile monomers to form triazine rings.[29] A careful selection of monomers allows us to design any desired functionalities into the backbone of the framework. Several CTFs have been used for selective adsorption of CO_2 and CH_4.[30] However, the adsorption of acetylene and ethylene has only been reported using CTF-PO71[31] that was synthesized from the Pigment Orange 71. The acetylene/ethylene separation was attributed to the pyrrolo-pyrrole aromatic unit in the framework. Due to the advantage of high surface area, porosity and control over the functionality, CTFs provide a good platform for olefin adsorption. In addition, CTFs are highly stable both thermally and chemically.[31,32]

Two dimensional CTFs are made using rigid aromatic units to provide stability and good pi-pi interaction for stacking into sheets.[34] Unsaturated aliphatic linkers could also provide good pi-pi interactions for the extended framework formation. However, the potential of such linkers to form COF structures has not been explored in detail. Ethylene dimer $(C_2H_2)_2$ has a large dispersion energy,[35] which can be utilized in a CTF structure. Additionally, the formation of triazine rings can provide extra support to form stable structures.[36] Recently, FUM-CTF was reported to selectively adsorb CO_2 because of the presence of ultramicropores and high nitrogen content.[30] The FUM-CTF material, which exhibited a high thermal and chemical stability, was made using fumaronitrile (aliphatic linker) as the monomer. Here, we propose the strategical design of a novel CTF (Hexene-CTF) using trans-3-hexenedinitrile as the monomer. The scope of this work is to obtain an olefin functionalized CTF that can selectively adsorb acetylene and ethylene over methane and provide enough stability for the framework formation. The additional benefits of a robust structure and higher nitrogen content allows olefin functionalized CTFs to be a good choice for selective acetylene and ethylene adsorption. Moreover, the commercial availability and cheap cost of the monomers allows an inexpensive alternative for the synthesis of a C_2H_2 and C_2H_4 selective microporous adsorbent.

Results and discussion

Synthesis and Characterization of Hexene-CTFs. The preparation of Hexene-CTF was carried out using the ionothermal synthesis approach in which trans-3-Hexenedinitrile was mixed with $ZnCl_2$ in quartz ampoules at different temperatures and different monomer to $ZnCl_2$ ratios (see detailed procedure in the supporting information). A continuous reversible trimerization of the nitrile groups occurs in the presence of molten $ZnCl_2$ at high temperatures which serves as a Lewis acid catalyst and as a solvent. An additional increase in temperature causes reorganization of the trimerized moieties into an extended framework which in principle is thermodynamically stable at the highest synthesis temperature.[29,32] A series of Hexene-CTF materials (scheme 1) was synthesized by varying the temperature (400°C and 500°C) and the molar ratio of linker to $ZnCl_2$ (1:1, 1:5 and 1:10). In the following, the resulting polymers are named as Hexene-CTF_x_y, where x = synthesis temperature and y = $ZnCl_2$ molar equivalents. The products were obtained as black monoliths which were crushed into powders for efficient cleaning using distilled water, 1M HCl (reflux) and tetrahydrofuran (THF). Thereafter, the materials were activated at 120°C under vacuum overnight prior to further analysis. The obtained yields were always >80%.

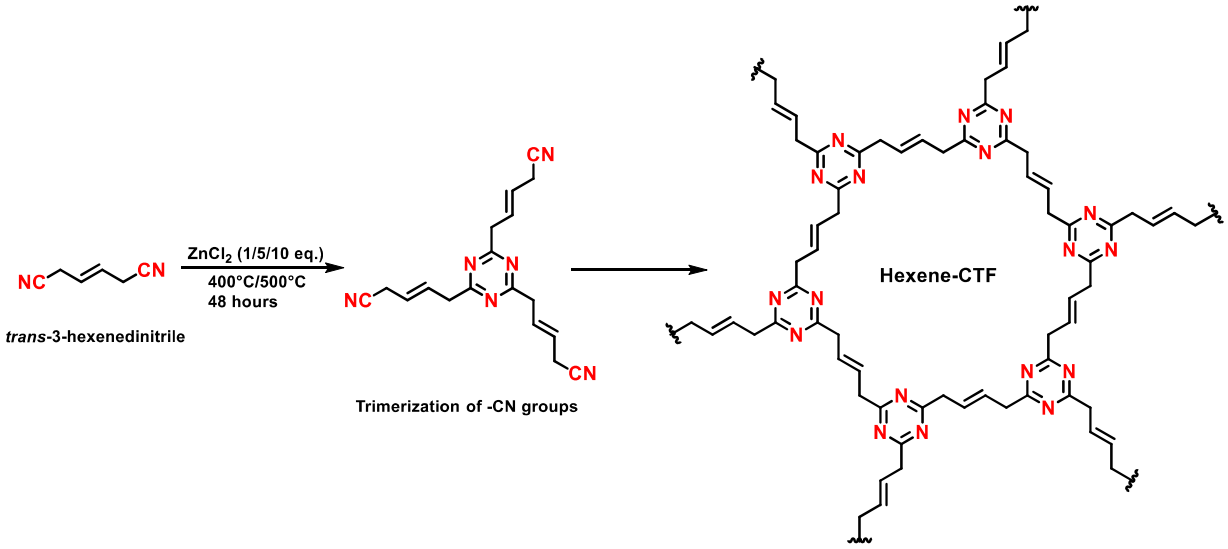

Scheme 1: Idealized representation of the formation of Hexene-CTF through the trimerization of trans-3-hexenedinitrile.

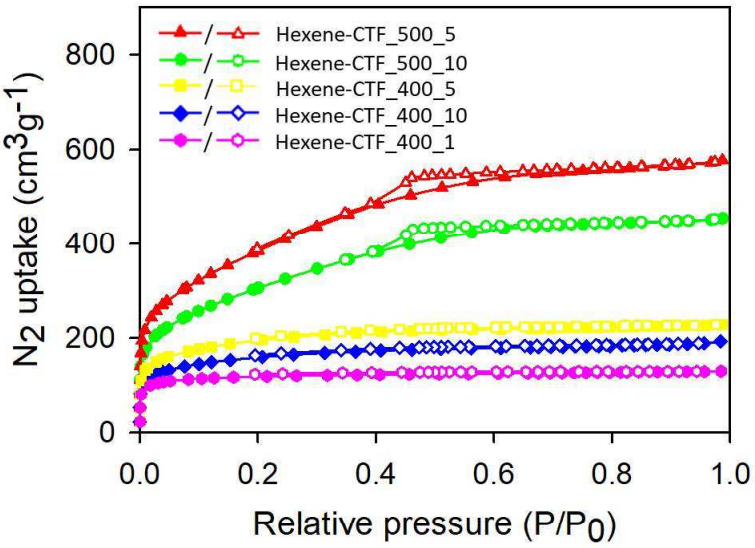

Figure 1: N_2 adsorption (closed symbols) and desorption (open symbols) isotherms of all Hexene-CTFs obtained at 77K.

The N_2 adsorption-desorption (Figure 1) isotherms of all the Hexene-CTF materials represent a Type I isotherm, which is typical for microporous materials and is a common feature of several CTFs.[37,38,39] Materials synthesized at 400°C are purely microporous. However, at higher synthesis temperatures (500°C), a hysteresis was observed which indicates the presence of mesoporosity. This is a common phenomenon observed in CTFs, where higher temperatures cause corrosive fragmentation of the walls on top of the micropores due to thermal decomposition.[32] This results

in the conversion of some of the micropores into mesopores (Figure S1). Table S1 lists the surface area and porosity characteristics of the produced Hexene-CTF series. The obtained surface areas were proportional to the synthesis temperatures. The monomer to $ZnCl_2$ ratio of 1:5 resulted in a higher surface area at both 400°C and 500°C. Increasing the $ZnCl_2$ up to 10 eq. reduced the surface area and increased the amorphous content. In addition, the elemental analysis results (table S2) correspond well to the N_2 uptake isotherms showing an increase in the carbon content with an increase in the synthesis temperature due to the C-C bond carbonization and C-H bond activation with H_2 evolution causing thermal decomposition of the materials.[40] Additionally, a decrease in the nitrogen content was observed at higher synthesis temperature due to the homolytic cleavage of -CN as previously reported for other CTFs.[28,29,32,40] For a particular synthesis temperature, the dependence of the carbon content on the monomer to $ZnCl_2$ ratio also corresponded to their surface areas, with higher C contents being associated with lower surface areas. The successful trimerization of the nitrile groups was confirmed through Fourier transform infra-red (FTIR) analysis (Figure 2) as evidenced by the typical triazine peaks around 1360 cm^{-1} and 1550 cm^{-1}.[41,42] Additionally, the FTIR spectra of the monomer does not contain these peaks suggesting that the framework consisted of triazine rings in all the materials. Furthermore, the -CN peak at 2226 cm^{-1} was completely attenuated corresponding to the absence of monomeric impurities and ensuring the complete conversion into triazine units.[43]

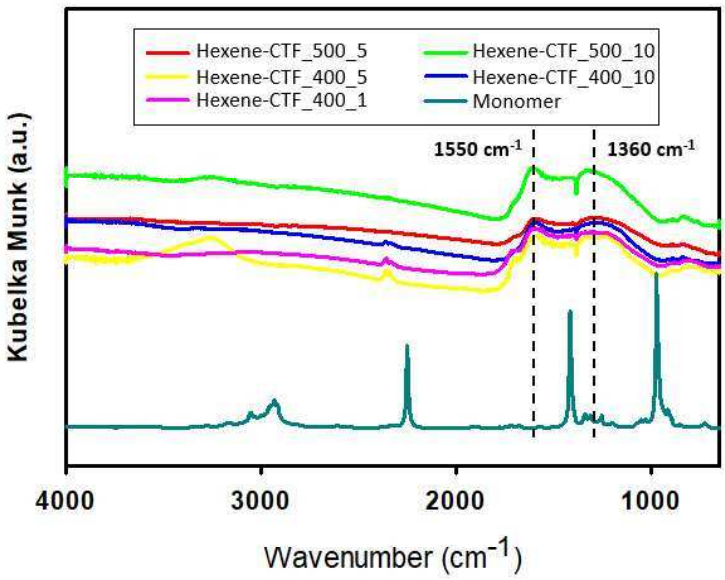

Figure 2: FT-IR spectra of all the Hexene-CTFs and the trans-3-hexenedinitrile monomer.

Structural and morphological analysis.

Powder X-ray diffraction (PXRD) measurements were performed to characterize the materials' phase and nature. All the CTFs showed characteristics of amorphous materials with a broad

diffraction band at 2θ = 26°, which can be assigned to a two-dimensional sheet stacking (Figure S2). This is a common feature observed in CTFs where due to the harsh synthesis conditions, the materials are mostly amorphous.[40,41,42] Interestingly, the diffraction for the Hexene-CTF_400_10 is broader whereas for the Hexene-CTF_400_1 it is relatively sharper and more intense. This indicates that the higher $ZnCl_2$ content increases the amorphous nature. Previously, it was observed that a 1:1 ratio of monomer:$ZnCl_2$ was optimal for complete trimerization, but when the $ZnCl_2$ content was increased, an enhanced surface area was observed.[32] However, we noticed that, there is a kind of trade-off between the order and the surface area of the material.

To explore this in more detail, TEM was used. In general, for all the Hexene-CTF materials several clusters displaying layered crystalline features dispersed amongst a larger amorphous region were seen (Figure 3). The clusters can be correlated to the hexagonal stacking of the 2D sheets. As expected, a higher number of crystalline clusters were observed for the Hexene-CTF_400_1 in comparison to Hexene-CTF_400_10 (Figure 4 and Figure S3). This is linked to the lower $ZnCl_2$ content that likely reduced nucleation and hence during growth led to fewer defects in the framework. The plane spacing showed an average of 0.34 nm for Hexene-CTF_400_1 and 0.35 nm for Hexene-CTF_400_10 corresponding to the broad PXRD peak around 2θ =26°. However, we also noticed several regions with a plane spacing of ~0.25 nm (Figure S4). This is likely due to the flexible nature of the aliphatic monomer causing distortion in the structure at high synthesis temperatures. Furthermore, a lower synthesis temperature ensured fewer carbonization defects, whereas at 500°C, the Hexene-CTF_500_10 exhibited a spaghetti-like network of lattice fringes within an amorphous bulk (Figure 4c and Figure S3c). Additionally, electron energy loss spectroscopy (EELS) measurements of the carbon K-edge of the materials confirmed the presence of a majority amorphous bulk. To study the influence of the synthesis temperature on the morphology of the materials, SEM measurements were collected (Figure S3). The average particle size is largest for Hexene-CTF_400_1, which has been shown to contain more crystalline clusters compared to other Hexene-CTFs made at higher temperatures and higher $ZnCl_2$ equivalents. For the higher synthesis temperature (Hexene-CTF_500_10), the average particle size decreases, which can be related to the increase in amorphous characteristics caused by defects at higher synthesis temperatures. This matches the trends in the surface area measurements, PXRD patterns and TEM analysis.

Bromine addition is a common technique used to estimate the degree of olefin unsaturation. Bromine gas is highly reactive towards the double bonds and forms C-Br bond easily. From the quantified increase in mass of the CTF after the bromination one can easily estimate the total number of accessible double bonds in the CTF material. For an ideal structure having no defects, the total bromine content should be 1.51 g/g. For the Hexene-CTF_400_10 only 3.91 mmol/g or 0.62 g/g bromine reacted, which means that only 41% of the double bonds are accessible after the CTF formation (Table S2). This is probably due to the harsh synthetic conditions in which partial carbonization occurs. Overall, the degree of unsaturation follows the order: Hexene-CTF_400_1 (46%) > Hexene-CTF_400_5 (44%) > Hexene-CTF_400_10 (41%) > Hexene-CTF_500_5 (39.7%) > Hexene-CTF_500_10 (39%).

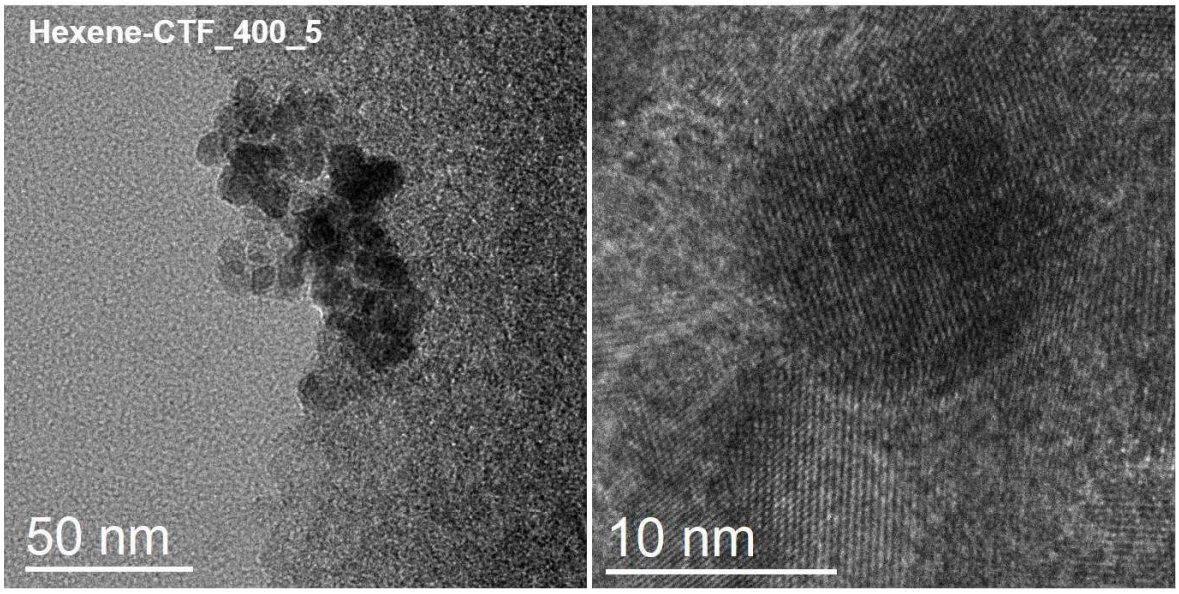

Figure 3: TEM image of Hexene-CTF_400_5 showing crystalline patches in amorphous bulk region.

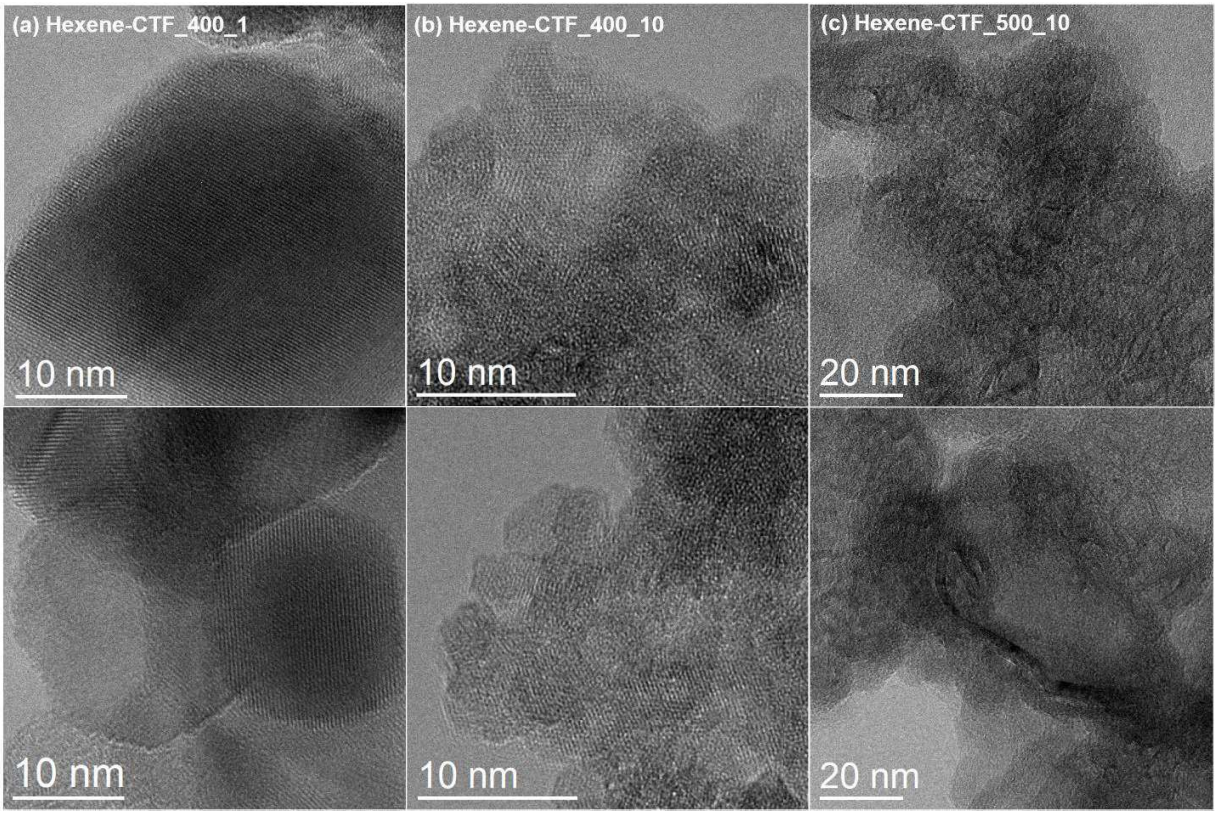

Figure 4: TEM images revealing the different structural arrangements of a) Hexene-CTF_400_1, b) Hexene-CTF_400_10 and c) Hexene-CTF_500_10.

The physicochemical stability of the Hexene-CTFs as studied by thermogravimetric analysis (TGA) revealed that all the CTFs high thermal stabilities from 425°C to 500°C after which they started to decompose (Figure S5). The materials are insoluble in common organic solvents such as acetone, methanol, ethanol, dichloromethane, tetrahydrofuran, dimethylformamide, dimethyl sulfoxide, diethyl ether and chloroform. In addition, the stability of the Hexene-CTF_500_5 was tested in boiling water for 3 days. The N_2 adsorption measurement after this treatment showed that the porosity of the material was retained (Figure S6).

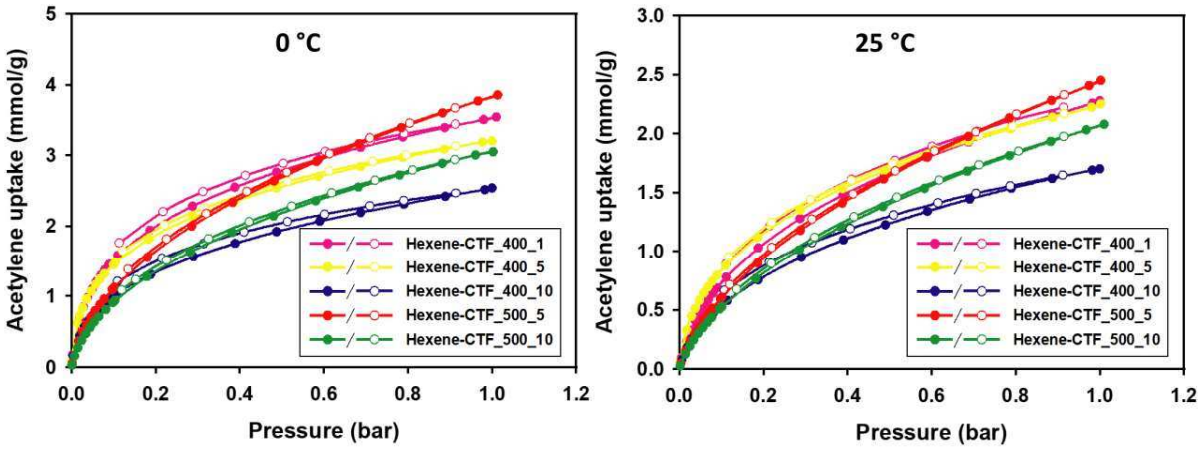

Figure 5: Acetylene adsorption (closed symbols) and desorption (open symbols) isotherms of all Hexene-CTFs obtained at 0°C and 25°C.

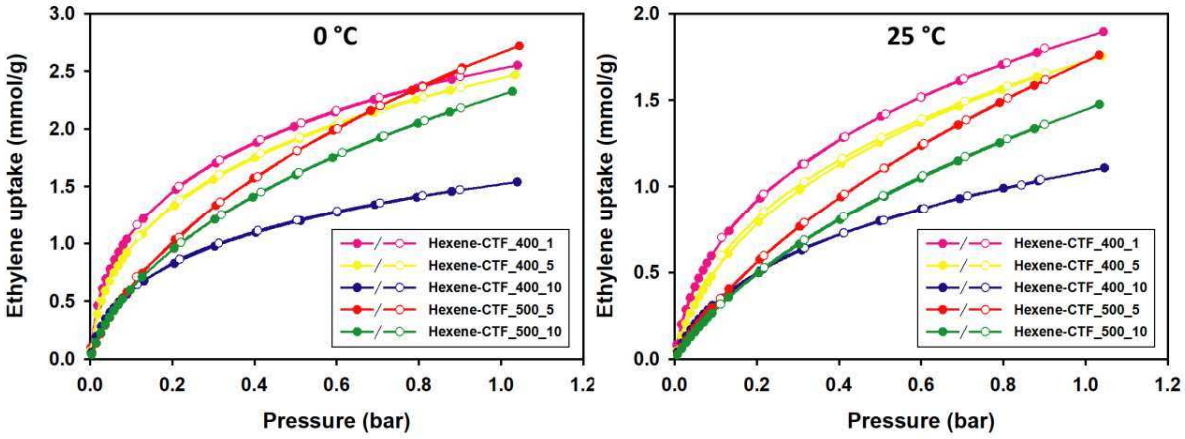

Figure 6: Ethylene adsorption (closed symbols) and desorption (open symbols) isotherms of all Hexene-CTFs obtained at 0°C and 25°C.

Selective olefin adsorption. We studied the targeted adsorption of C_2H_2 and C_2H_4 on the Hexene-CTFs by utilizing the presence of inherent olefin functionalities in the CTFs (Table S3, Figures 5 and 6). The highest C_2H_2 uptake of 3.85 mmol/g was obtained using the Hexene-CTF_500_5 at

0°C and 1 bar. The second highest C_2H_2 uptake was 3.54 mmol/g using Hexene-CTF-400_1 at 0°C and 1 bar. Even though the surface area of Hexene-CTF_400_1 is much lower than Hexene-CTF_500_5, the C_2H_2 uptake is quite close. This can be attributed to the higher ordering in Hexene-CTF_400_1, resulting in an enhanced interaction of the C_2H_2 gas molecules with the framework. Particularly, in the lower pressure regime, where the adsorption is dominated by the interaction between the chemical moieties rather than the physical adsorption alone, the Hexene-CTFs synthesized at 400°C outperforms the Hexene-CTFs synthesized at 500°C. This is also can be corroborated by the degree of unsaturation retained in the CTFs as a function of temperature. Hexene-CTF_400_1 retained 46% of the double bonds (estimated by the bromine number, Table S2), after the harsh synthesis conditions, which is a higher content compared to Hexene-CTF_500_5 (39.7% double bonds) in which more carbonization occurs. The same trend is also observed for the C_2H_4 adsorption for which Hexene-CTF_400_1 exhibits a higher C_2H_4 uptake in the low-pressure regime in comparison to Hexene-CTF_500_5. The unsaturated gases and the olefin functionalities present within the CTF framework exhibit pi-pi interactions which results in a higher C_2 gas uptake compared to C_1 gas. We cannot rule out the partial contribution of physisorption during the gas uptake in these materials. However, the variation in the ordering of the materials and the resulting olefin gas uptake values prove that the pi-pi interaction between C_2H_2/C_2H_4 molecules and the alkene functionality of Hexene-CTF is a more dominant factor than physisorption.

The selectivity over CH_4 was estimated using the ratio of the initial slopes in the Henry regime of the adsorption isotherms (Table 1 and Figures S7-S10). These initial slopes were obtained by a linear fit. In Table 1 the estimated C_2H_2/CH_4 and C_2H_4/CH_4 selectivities of the Hexene-CTF family are presented. In general, the selectivities for the Hexene-CTFs vary between 14.5-24.5 (C_2H_2/CH_4) and 9.4-14.8 (C_2H_4/CH_4). There is apparently no direct correlation with the applied synthesis conditions. The CH_4-alkene pi-H interaction is weaker in comparison to the CH_4-aromatic pi-H interaction,[44] which is beneficial for a higher selectivity. In a purely aromatic CTF, the pi-H interaction influences the C_2/C_1 selectivity negatively, whereas the presence of aliphatic olefin components helps by having a reduced interaction with CH_4 and thus increases the C_2/C_1 selectivity. Noteworthy is that the alkene functionality-CH_4 interaction cannot be termed as a pi-H interaction, however, the presence of both benzene and ethylene groups can result in pi-H interactions.[44] Unlike the C_2H_4-aromatic unit interaction, the C_2H_4-aliphatic pi-pi interaction is dominated by dispersion energy.[35] To better understand the adsorption properties of the Hexene-CTF for C_2H_4, the isosteric heats of adsorption (Q_{st}) were calculated using the Clausius-Clapeyron equation for the isotherms measured at 0°C and 25°C. The Q_{st} values range from 26-47 kJ/mol for C_2H_2 (Figure S11) and 24-37 kJ/mol for C_2H_4 (Figure S12), which is significantly higher than several other reported porous materials. Especially, the CTF-PO71 material showed a good C_2H_2/C_2H_4 selectivity but had lower Qst values than Hexene-CTFs.[31] The obtained values highlight the importance of introducing olefin functionalities in the Hexene-CTFs, which provides efficient pi-pi complexation between the framework and the adsorbed unsaturated gas molecules. In addition, the Q_{st} for methane is lower and ranges from 14-21 kJ/mol (Figure S13), which validates

the selective adsorption of C_2H_2 and C_2H_4 over CH_4. The Q_{st} values are higher for the Hexene-CTFs made at 400°C and decrease for Hexene-CTFs made at 500°C due to higher number of defects caused in the framework by the higher reaction temperature. Such difference is also seen in previous cases of CTFs for CO_2 adsorption. The selectivities are in the mid-range compared to several other porous materials. Mostly MOFs have been studied for such separations and the presence of metals in these materials plays a major role in the selectivity. However, some of these materials have a lower overall gas uptake [17] and are also less stable than CTFs. Here we present for the first time the use of a metal-free adsorbent having inherent aliphatic functional groups for such C_2/C_1 separation. Furthermore, this is the first report of using COFs for C_2H_2/CH_4 and C_2H_4/CH_4 selectivity studies.

Selective CO_2 adsorption. In addition to the C_2/C_1 separation, we also examined the materials for their CO_2 uptake. The CO_2 adsorption/desorption isotherms were recorded at 0°C and 25°C up to 1 bar (figure 7). The detailed uptake values are given in Table S3. Upon comparison of these values with respect to the synthesis conditions, the Hexene-CTF_400_1 shows the highest CO_2 uptake of 2.66 mmol/g (0°C, 1 bar) and 1.72 mmol/g (25°C, 1 bar). These uptakes are amongst the average when compared to previously reported CTFs.[27] This is due to a lower N content than most other CTFs which is essential for increasing the interaction with CO_2. The highest uptake for the Hexene-CTF was also observed for the material synthesized at 400°C. This is in contradiction with most of the reported CTFs for CO_2 adsorption, where the CTF made at higher synthesis temperature usually shows the highest CO_2 uptake because of a higher surface area (physisorption) dominating the overall adsorption.[30] However, in the case of Hexene-CTFs, the CO_2 adsorption is more related to the presence of the functional groups rather than just physisorption. Based on the elemental analysis (table S2), the Hexene-CTF_400_1 has the highest N content resulting in a higher CO_2 uptake. This further emphasizes the importance of having a large N content for CO_2 interaction. The amount of $ZnCl_2$ used for the synthesis also had an influence on the CO_2 adsorption. More specifically, an increase in the $ZnCl_2$ equivalents decreased the overall CO_2 uptake. We attribute this to be a result of some residual Zn present in the materials which could not be removed even after extensive washing. The Zn residue decreases the surface area and blocks the interaction sites with CO_2. The Clausius-Clapeyron equation was used to calculate the isosteric heat of adsorption (Q_{st}) of CO_2 using the isotherms at 0°C and 25°C (Figure S14). The highest Q_{st} of 32.2 is calculated for Hexene-CTF_400_1 and it supports the corresponding highest CO_2 uptake amongst the Hexene-CTF family. The liquefaction heat of bulk CO_2 is 17 kJ/mol[42] and the Q_{st} values for the Hexene-CTFs are much higher (~27-32 kJ/mol). These values are also higher than those for activated carbon at low CO_2 pressure (17.8 kJ/mol) and is well above the Qst values of several CTFs.[30]

Table 1: The gas selectivities of Hexene-CTFs in comparison to selected other porous materials.

Material description	Temperature (°C)	C_2H_2/CH_4	C_2H_4/CH_4	CO_2/N_2	CO_2/CH_4
Hexene-CTF_400_10	25	22.3	13.6	82.5	7.5
	0	21.8	13.2	67.9	9.8
Hexene-CTF_400_5	25	18.9	10.3	44.5	7.8
	0	20.6	10.8	45.6	8.3
Hexene-CTF_400_1	25	14.5	12.8	44.8	8
	0	16.3	11.8	44.6	8.6
Hexene-CTF_500_10	25	22.8	11.3	25.2	7
	0	24.5	14.8	29.6	9.6
Hexene-CTF_500_5	25	19.4	9.4	25.8	5.3
	0	19.9	10	29.2	6.6
UTSA-33a[45]	23	13.8	11.1	-	-
	0	16.1	14.7	-	-
ZJU-61a[46]	25	74.4	49.5	-	-
	0	115.3	87.6	-	-
UTSA-10a[47]	23	8.1	4.6	-	-
HOF-BTB[48]	25	7.8	7.9	-	-
	0	9.5	9.3	-	-
Wet ZIF-8[18]	0	-	5.56	-	-
ZIF-67/water-ethylene glycol slurry[19]	0	-	10	-	-
Solid ZIF-67[19]	0	-	3.1	-	-

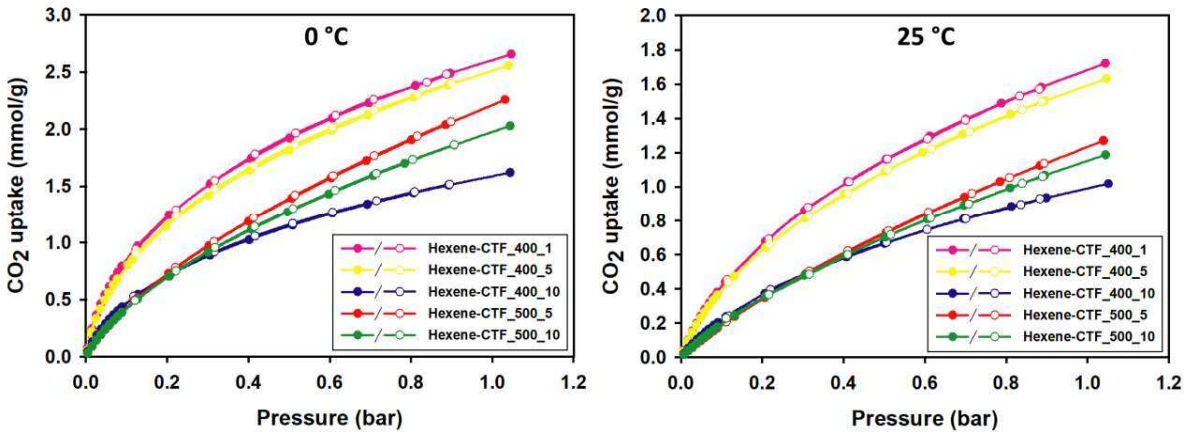

Figure 7: CO_2 adsorption (closed symbols) and desorption (open symbols) isotherms of all Hexene-CTFs obtained at 0°C and 25°C.

The selectivity of the CTFs for CO_2 over CH_4 and N_2 was also studied as it is an important factor for carbon capture and storage (figures S16-S19).[26,27] The selectivity of all the materials is presented in Table 1. The CO_2/N_2 selectivity was calculated using the slopes ratio in the Henry regime of the CO_2 (<0.05 bar) and N_2 (<0.1 bar) adsorption isotherms. For porous materials like MOFs and porous organic frameworks (POFs), this is a common method to estimate the gas separation performance; the CO_2/N_2 selectivity is among the top 15% for several porous organic polymers.[30] As expected the selectivity is higher for the materials synthesized at 400°C than at 500°C due to the higher number of functional groups remaining in the material. From this study, it can be concluded that for Hexene-CTFs, the synthesis temperature has a role in the selectivity of CO_2 over N_2 with 400°C to be the better one. However, the employed amount of $ZnCl_2$ has negligible effects towards the selectivity. In addition, Hexene-CTF performs well in comparison to several other porous organic polymers in terms of CO_2/CH_4 selectivity.[30]

Conclusion:

In conclusion, for the first time, a family of aliphatic olefin functionalized covalent triazine framework materials were synthesized using the ionothermal synthesis method. The Hexene-CTFs showed tunable textural and porous properties that is a result of varying synthesis temperature and monomer:$ZnCl_2$ ratio. The surface areas for the materials synthesized at 500°C were higher than for the materials synthesized at 400°C due to an increase in the number of defects causing mesoporosity in addition to the expected microporosity. High resolution imaging of the material revealed that Hexene-CTFs consisted of clusters of crystalline regions embedded in an amorphous bulk. The size of these crystalline regions depended on the synthesis temperatures and the employed $ZnCl_2$ equivalents. The Hexene-CTF_400_1 showed the largest crystalline clusters due to the usage of a lower amount of $ZnCl_2$ and a lower synthesis temperature, whereas, the Hexene-CTF_500_10 was characterized by spaghetti-like lattice planes. The C_2H_2, C_2H_4 and CO_2 gas adsorption revealed that the adsorption performance

depended more on the materials' structural order than the surface area. In the low-pressure regime, the higher ordered crystalline CTFs showed a higher adsorption of C_2H_2, C_2H_4 and CO_2 even though it had the least surface area due to higher availability of functional groups in the framework. This also had an influence on the selectivity over CH_4 (for C_2H_2, C_2H_4 and CO_2) and N_2 (for CO_2). Though the general uptake for CO_2 is average compared to several other CTFs, the selectivities are among the highest in comparison to several other porous organic polymers. Furthermore, this is the first time where the concept of using aliphatic unsaturated functional groups in the framework of a COF is used to adsorb unsaturated gases selectively by utilizing higher pi-pi interaction. This notion can be extended to design intricate COFs which can further improve the adsorption properties.

Materials and methods.

Instrumentation: The chemicals were purchased from Sigma-Aldrich and used without further purifications unless mentioned otherwise. Elemental analyses (C/H/N/O) were performed on a Thermo Scientific Flash 2000 CHNS-O analyzer equipped with a TCD detector. N_2 adsorption isotherms were obtained from a Belsorp Mini apparatus at 77K. Fourier transform infrared spectroscopy (FT-IR) was carried out in a Thermo Nicolet 6700 FTIR spectrometer equipped with a nitrogen cooled MCT detector and a KBr beam splitter for the region of 4000-650 cm^{-1}. X-Ray powder diffraction (XRPD) measurements were done on a Thermo Scientific ARL X'Tra diffractometer, operated at 40 kV, 30 mA using Cu Kα radiation (λ = 1.5406 Å). Carbon dioxide (CO_2), Ethlyene (C_2H_4), Acetylene (C_2H_2), Methane (CH_4) and Nitrogen (N_2) gas adsorption isotherms were collected using a Quantachrome iSorb-HP gas sorption analyzer. Thermogravimetric analysis (TGA) was performed on a Netzsch STA-449 F3 Jupiter-simultaneous TG-DSC analyzer within a temperature range of 20-800°C, under a N_2 atmosphere and heating rate of 2°C/min. 1800-2700 scans were further accumulated with a 4 s recycle delay. Scanning electron microscopy (SEM) images were taken on a FEI Quanta 200 FEG microscope with 4 nm resolution operating at 30 kV. Transmission electron microscopy (TEM) images were acquired on a FEI Tecnai G2 F20 X-Twin FEG TEM operated at 200 kV and equipped with a Gatan Imaging Filter (GIF) Tridiem™.

Synthesis of Hexene-CTFs: The targeted Hexene-CTF materials were synthesized using the monomer, trans-3-hexenedinitrile under ionothermal conditions. In general, trans-3-hexenedinitrile (106 mg, 1 mmol) was charged in an ampoule with 1/5/10 equivalents of $ZnCl_2$ in a glovebox. The ampoule was then evacuated, flame-sealed and slowly heated to the desired temperature (400°C /500°C) with a heating rate of 1°C/min for 48 hours in a Nabertherm furnace oven. Once the oven was cooled to room temperature, the ampoules were opened, and the crude material was grounded and washed with distilled water (stirring for 12 hours) to remove unreacted $ZnCl_2$. Then it was refluxed with 0.1 M HCl and THF for 12 hours each to remove water and unreacted linker/organic impurities. The final product was activated at 120°C under vacuum for 24 hours.

Bromine addition reaction: In general, to quantify the number of double bonds present in the Hexene-CTFs, 100 mg of the CTF was weighed in a dry Schlenk flask and treated with an excess amount of bromine gas under inert atmosphere. The accessible unsaturated olefin bonds in the material were brominated whereas the unreacted bromine was eliminated by heating the material at 120°C under vacuum.[33] After removal of unreacted bromine gas, the increase in the mass of the CTF was calculated to estimate the amount of bromine reacted to the CTF.

Acknowledgements

C.K. acknowledges the support from the Research Board of Ghent University (GOA010-17, BOF GOA2017000303). H.S.J. thanks FWO [PEGASUS]2 Marie Sklodowska-Curie grant agreement No 665501 for Incoming postdoctoral fellowship. H.M.F. and L.G.B. acknowledge funding through the Helmholtz Recruiting Initiative (award number I-044-16-01).

References

1. O. Colten, *Industrial & Engineering Chemistry*, 1959, **51(9)**, 983-984.

2. L. A. Falligant, U.S. Patent 2683484, 1954.

3. A. Moshonov, Y. Avny, *Journal of Applied Polymer Science*, 1980, **25**, 771-781.

4. G. Parker, L. Smith, I. Baxendale, *Tetrahedron*, 2016, **72**, 1645-1652.

5. S. P. Robinson, U.S. Patent 2482438, 1949.

6. H. A. Dutcher, U.S. Patent 2582016, 1946.

7. Beyond the Ethylene Steam Cracker, www.acs.org/content/acs/en/pressroom/cutting-edge-chemistry/beyond -the-ethylene-steam-cracker.html, (accessed Nov 5, 2018).

8. Ethene (Ethylene), www.essentialchemicalindustry.org/chemicals/ethene.html, (accessed Nov 5, 2018).

9. Cracking and related refinery processes, www.essentialchemicalindustry.org/processes/cracking-isomerisation-and-reforming.html#steam_cracking, (accessed Nov 5, 2018).

10. E. A. Kaufman, J. A. Moss, J. L. Jr. Pickering, U.S. Patent 5372009, 1994.

11. P. F. Keusenkothen, F. Hershkowitz, WO2012/0099679A1, 2012.

12. C. Millet, P. Bourgeois, G. Kraus, J.-P. Gabillard, U.S. Patent 6270557B1, 2001.

13. L. Zhang, X. Cui, H. Xing, Y. Yang, Y. Cui, B. Chen, G. Qian, *RSC Advances*, 2017, **7**, 20795-20800.

14. M. Eddaoudi, D. Moler, H. Li, B. Chen, T. Reineke, M. O'Keeffe, O. Yaghi, *Accounts of Chemical Research*, 2001, **34**, 319-330.

15. J. Pang, F. Jiang, M. Wu, C. Liu, K. Su, W. Lu, D. Yuan, M. Hong, *Nature Communications*, 2015, **6**.

16. K. Liu, D. Ma, B. Li, Y. Li, K. Yao, Z. Zhang, Y. Han, Z. Shi, *J. Mater. Chem. A*, 2014, **2**, 15823-15828.

17. L. Zhang, X. Cui, H. Xing, Y. Yang, Y. Cui, B. Chen, G. Qian, *RSC Advances*, 2017, **7**, 20795-20800.

18. X. Zhang, P. Xiao, C. Zhan, B. Liu, R. Zhong, L. Yang, C. Sun, H. Liu, Y. Pan, G. Chen, *Industrial & Engineering Chemistry Research*, 2015, **54**, 7890-7898.

19. Y. Pan, C. Jia, B. Liu, Z. Zhang, X. Tong, H. Li, Z. Li, R. Ssebadduka, C. Sun, L. Yang, *Fluid Phase Equilibria*, 2016, **414**, 14-22.

20. S. Xiang, W. Zhou, J. Gallegos, Y. Liu, B. Chen, *Journal of the American Chemical Society*, 2009, **131**, 12415-12419.

21. Y. Zhang, B. Li, R. Krishna, Z. Wu, D. Ma, Z. Shi, T. Pham, K. Forrest, B. Space, S. Ma, *Chemical Communications*, 2015, **51**, 2714-2717.

22. Y. Khabzina, J. Dhainaut, M. Ahlhelm, H. Richter, H. Reinsch, N. Stock, D. Farrusseng, *Industrial & Engineering Chemistry Research*, 2018, **57**, 8200-8208.

23. H. Reinsch, *European Journal of Inorganic Chemistry*, 2016, 4290-4299.

24. K. Leus, T. Bogaerts, J. De Decker, H. Depauw, K. Hendrickx, H. Vrielinck, V. Van Speybroeck, P. Van Der Voort, *Microporous and Mesoporous Materials*, 2016, **226**, 110-116.

25. D. Aaron, C. Tsouris, *Separation Science and Technology*, 2005, **40**, 321-348.

26. L. Zhu, Y. Zhang, *Molecules*, 2017, **22**, 1149.

27. Y. Zeng, R. Zou, Y. Zhao, *Advanced Materials*, 2016, **28**, 2855-2873.

28. K. Sakaushi, M. Antonietti, *Accounts of Chemical Research*, 2015, **48**, 1591-1600.

29. P. Kuhn, M. Antonietti, A. Thomas, *Angewandte Chemie International Edition*, 2008, **47**, 3450-3453.

30. K. Wang, H. Huang, D. Liu, C. Wang, J. Li, C. Zhong, *Environmental Science & Technology*, 2016, **50**, 4869-4876.

31. Y. Lu, J. He, Y. Chen, H. Wang, Y. Zhao, Y. Han, Y. Ding, *Macromolecular Rapid Communications*, 2017, **39**, 1700468.

32. P. Kuhn, A. Forget, D. Su, A. Thomas, M. Antonietti, *Journal of the American Chemical Society*, 2008, **130**, 13333-13337.

33. S. Clerick, E. De Canck, K. Hendrickx, V. Van Speybroeck, P. Van Der Voort, *Green Chemistry*, 2016, **18**, 6035-6045.

34. W. Zhao, L. Xia, X. Liu, *CrystEngComm*, 2018, **20**, 1613-1634.

35. K. Kim, S. Karthikeyan, N. Singh, *Journal of Chemical Theory and Computation*, 2011, **7**, 3471-3477.

36. K. Schwinghammer, S. Hug, M. Mesch, J. Senker, B. Lotsch, *Energy & Environmental Science*, 2015, **8**, 3345-3353.

37. P. Katekomol, J. Roeser, M. Bojdys, J. Weber, A. Thomas, *Chemistry of Materials*, 2013, **25**, 1542-1548.

38. S. Dey, A. Bhunia, H. Breitzke, P. Groszewicz, G. Buntkowsky, C. Janiak, *Journal of Materials Chemistry A*, 2017, **5**, 3609-3620.

39. S. Dey, A. Bhunia, I. Boldog, C. Janiak, *Microporous and Mesoporous Materials* 2017, **241**, 303-315.

40. D. Osadchii, A. Olivos-Suarez, A. Bavykina, J. Gascon, *Langmuir*, 2017, **33**, 14278-14285.

41. G. Wang, K. Leus, H. Jena, C. Krishnaraj, S. Zhao, H. Depauw, N. Tahir, Y. Liu, P. Van Der Voort, *Journal of Materials Chemistry A*, 2018, **6**, 6370-6375.

42. H. Jena, C. Krishnaraj, G. Wang, K. Leus, J. Schmidt, N. Chaoui, P. Van Der Voort, *Chemistry of Materials*, 2018, **30**, 4102-4111.

43. G. Wang, K. Leus, S. Zhao, P. Van Der Voort, *ACS Applied Materials & Interfaces*, 2017, **10**, 1244-1249.

44. P. Tarakeshwar, H. Choi, K. Kim, *Journal of the American Chemical Society*, 2001, **123**, 3323-3331.

45. M. Das, H. Xu, S. Xiang, Z. Zhang, H. Arman, G. Qian, B. Chen, *Chemistry - A European Journal*, 2011, **17**, 7817-7822.

46. X. Duan, Q. Zhang, J. Cai, Y. Cui, C. Wu, Y. Yang, G. Qian, *Microporous and Mesoporous Materials*, 2014, **190**, 32-37.

47. Y. He, C. Song, Y. Ling, C. Wu, R. Krishna, B. Chen, *APL Materials*, 2014, **2**, 124102.

48. T. Yoon, S. Baek, D. Kim, E. Kim, W. Lee, B. Singh, M. Lah, Y. Bae, K. Kim, *Chemical Communications*, 2018, **54**, 9360-9363.

Table of contents entry

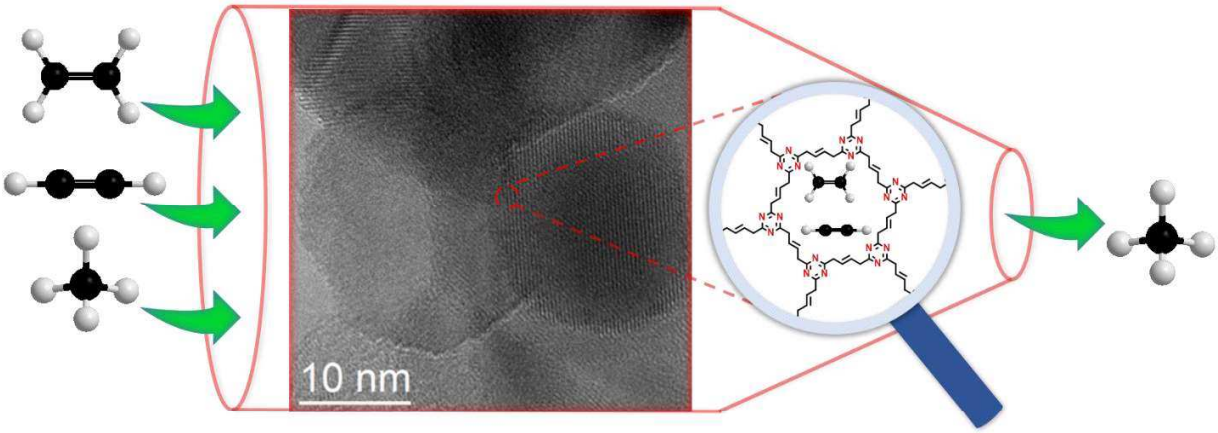

Aliphatic Hexene-Covalent triazine framework for C_2/C_1 hydrocarbon separation - dependence on morphology

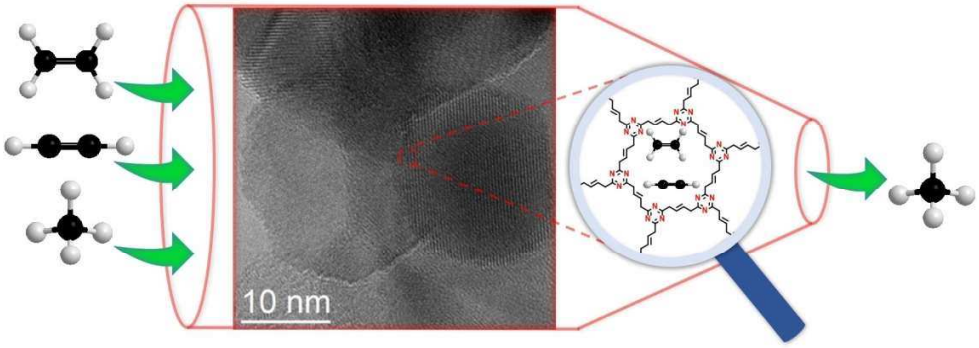

279x100mm (150 x 150 DPI)

Supplementary Information

An aliphatic Hexene-Covalent Triazine Framework for Selective Acetylene/Methane and Ethylene/Methane Separation

Chidharth Krishnaraj[1], Himanshu Sekhar Jena[1], Karen Leus[1], Helen M. Freeman[2], Liane G. Benning[2,3,4], Pascal Van Der Voort[1]*

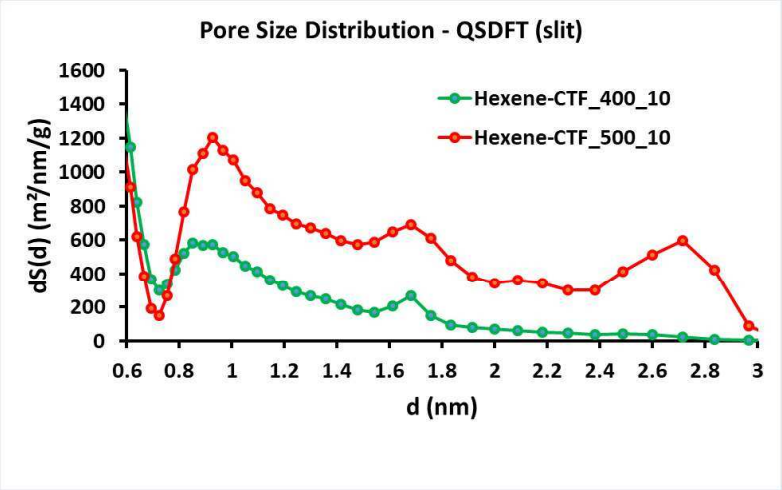

Figure S1: Pore size distribution of Hexene-CTF_400_10 and Hexene-CTF_500_10.

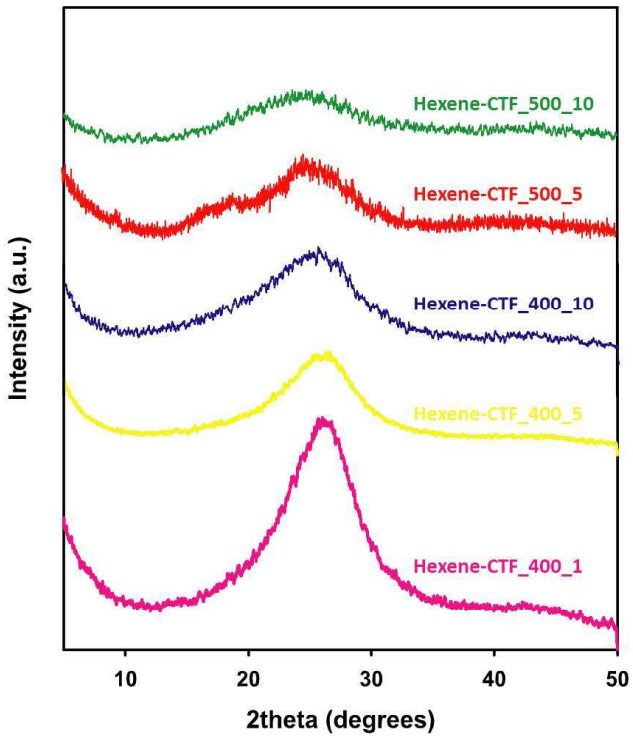

Figure S2: Powder X-Ray Diffraction (PXRD) patterns of all Hexene-CTFs.

Table S1: Porous properties of Hexene-CTFs

Material description	[a]S.A.$_{BET}$ ($m^2\ g^{-1}$)	[b]V_{micro} ($cm^3\ g^{-1}$)	[c]V_{tot} ($cm^3\ g^{-1}$)	V_{micro}/V_{tot} (%)
Hexene-CTF_400_10	499	0.2802	0.298	94.02
Hexene-CTF_400_5	579	0.3239	0.3413	94.90
Hexene-CTF_400_1	356	0.1965	0.2005	98.00
Hexene-CTF_500_10	1016	0.6437	0.6925	92.95
Hexene-CTF_500_5	1375	0.8293	0.8922	92.95

[a] BET surface area was calculated over the relative pressure range of 0.05–0.3 at 77 K. [b] V_{micro}, micropore volume was calculated by N_2 adsorption isotherms using the t-plot method. [c] V_{tot}, total pore volume was calculated at P/P0 = 0.98.

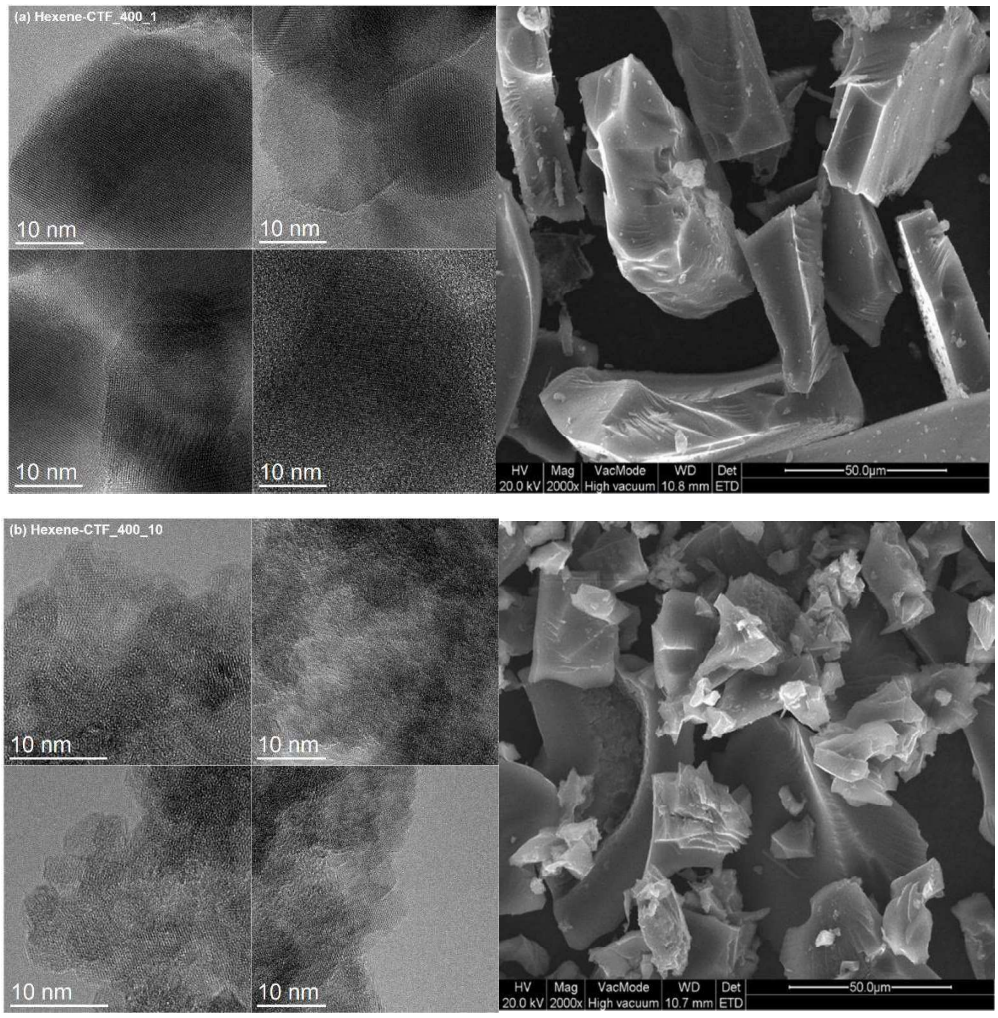

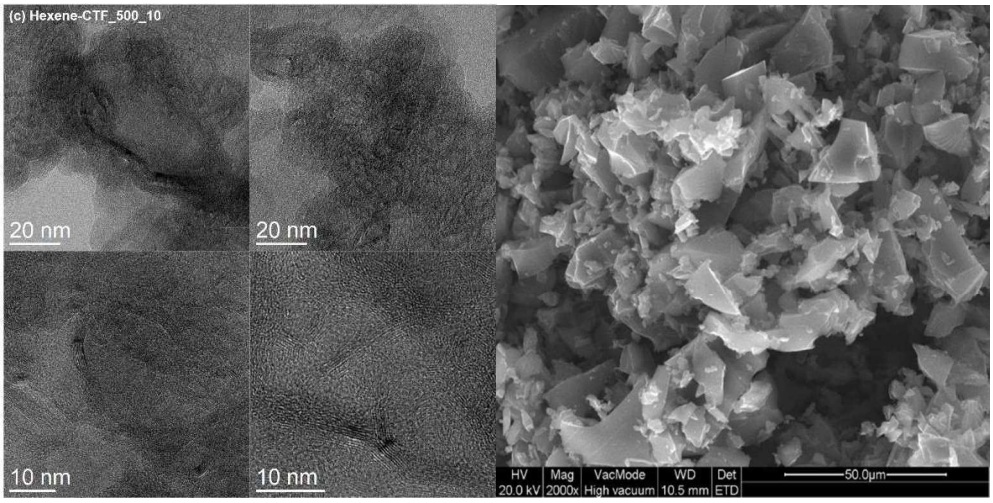

Figure S3: HR-TEM and SEM images of (a) Hexene-CTF_400_1, (b) Hexene-CTF_400_10 and (c) Hexene-CTF_500_10.

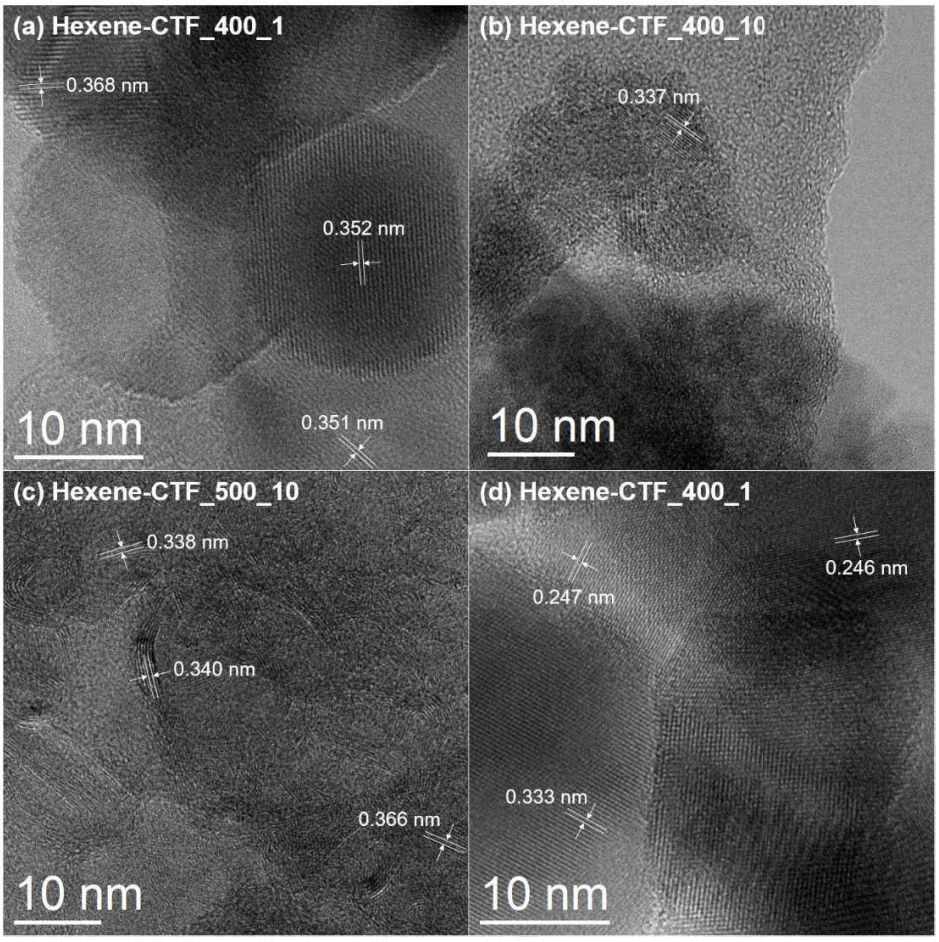

Figure S4: HR-TEM image of Hexene-CTF_400_1 showing two different plane-spacing.

Table S2: Elemental analysis (C/H/N) and Bromine number of all Hexene-CTFs.

Material description	C (wt. %)	H (wt. %)	N (wt. %)	Residue (wt. %)	Br number double bonds	C/N ratio
Hexene-CTF_400_10	70.9	1.9	8.8	18.3	0.62 g/g (41%)	8.05
Hexene-CTF_400_5	68.9	2.6	9.5	19	0.67 g/g (44%)	7.25
Hexene-CTF_400_1	66.1	2.8	11.1	20	0.69 g/g (46%)	5.95
Hexene-CTF_500_10	73.7	1.5	8.4	16.4	0.59 g/g (39%)	8.77
Hexene-CTF_500_5	70.7	1.5	8.7	19.1	0.60 g/g (39.7%)	8.12
Theoretical	67.9	5.7	26.4	-	1.51 g/g (100%)	2.57

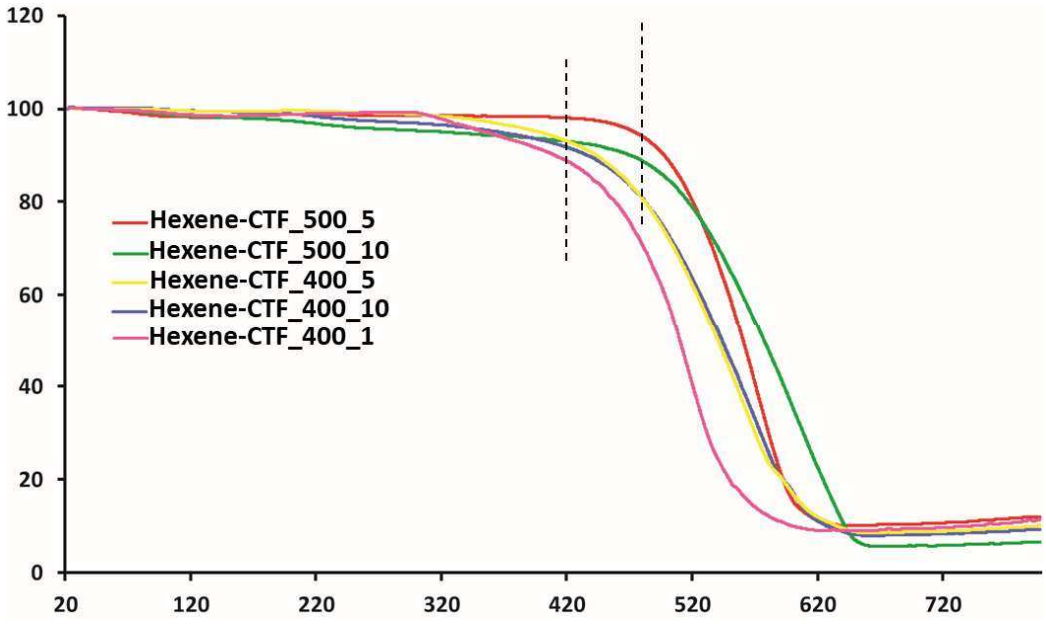

Figure S5: Thermogravimetric analysis (TGA) of all Hexene-CTFs.

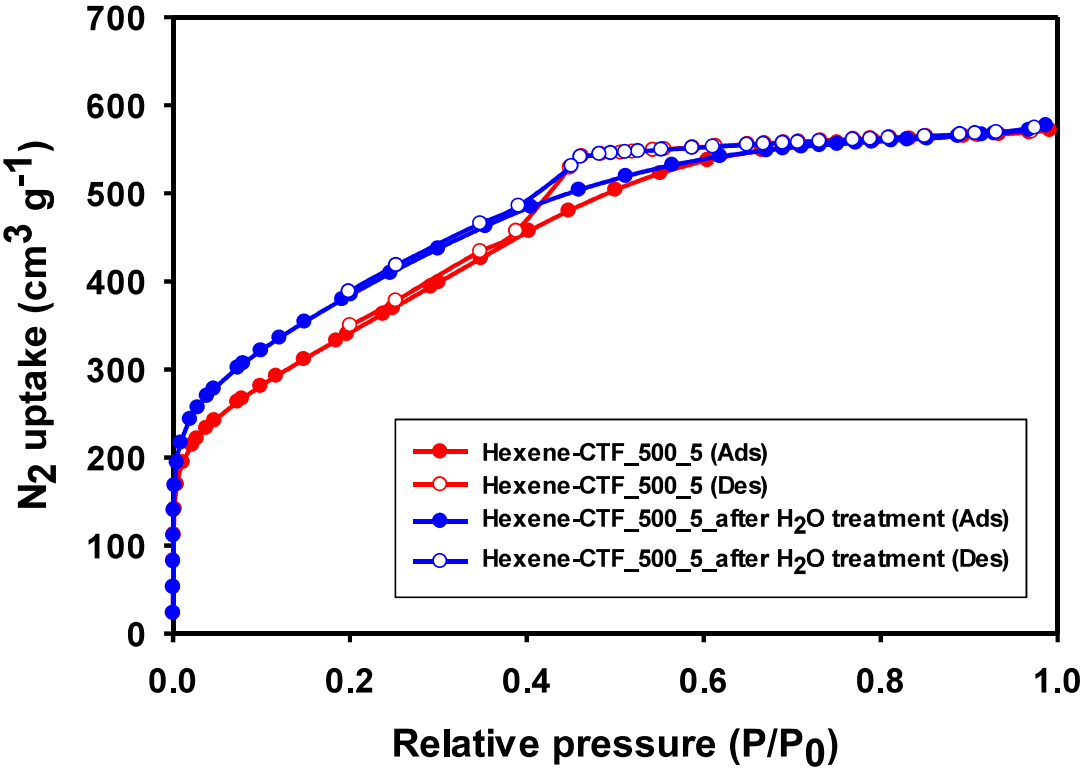

Figure S6: N_2 sorption isotherms of Hexene-CTF_500_5 before and after boiling water treatment.

Table S3: CO_2, N_2, CH_4, C_2H_4 and C_2H_2 gas uptakes by Hexene-CTFs at 25°C and 0°C at 1 bar.

Material description	Temp (°C)	CO_2 (mmol/g)	N_2 (mmol/g)	CH_4 (mmol/g)	C_2H_4 (mmol/g)	C_2H_2 (mmol/g)
Hexene-CTF_400_10	25	1.02	0.048	0.25	1.12	1.69
	0	1.62	0.091	0.4	1.54	2.54
Hexene-CTF_400_5	25	1.63	0.13	0.45	1.75	2.24
	0	2.56	0.21	0.72	2.47	3.19
Hexene-CTF_400_1	25	1.72	0.13	0.46	1.89	2.28
	0	2.66	0.24	0.74	2.55	3.54
Hexene-CTF_500_10	25	1.18	0.09	0.28	1.48	2.08
	0	2.03	0.16	0.43	2.33	3.05
Hexene-CTF_500_5	25	1.27	0.11	0.36	1.76	2.45
	0	2.26	0.17	0.61	2.72	3.85

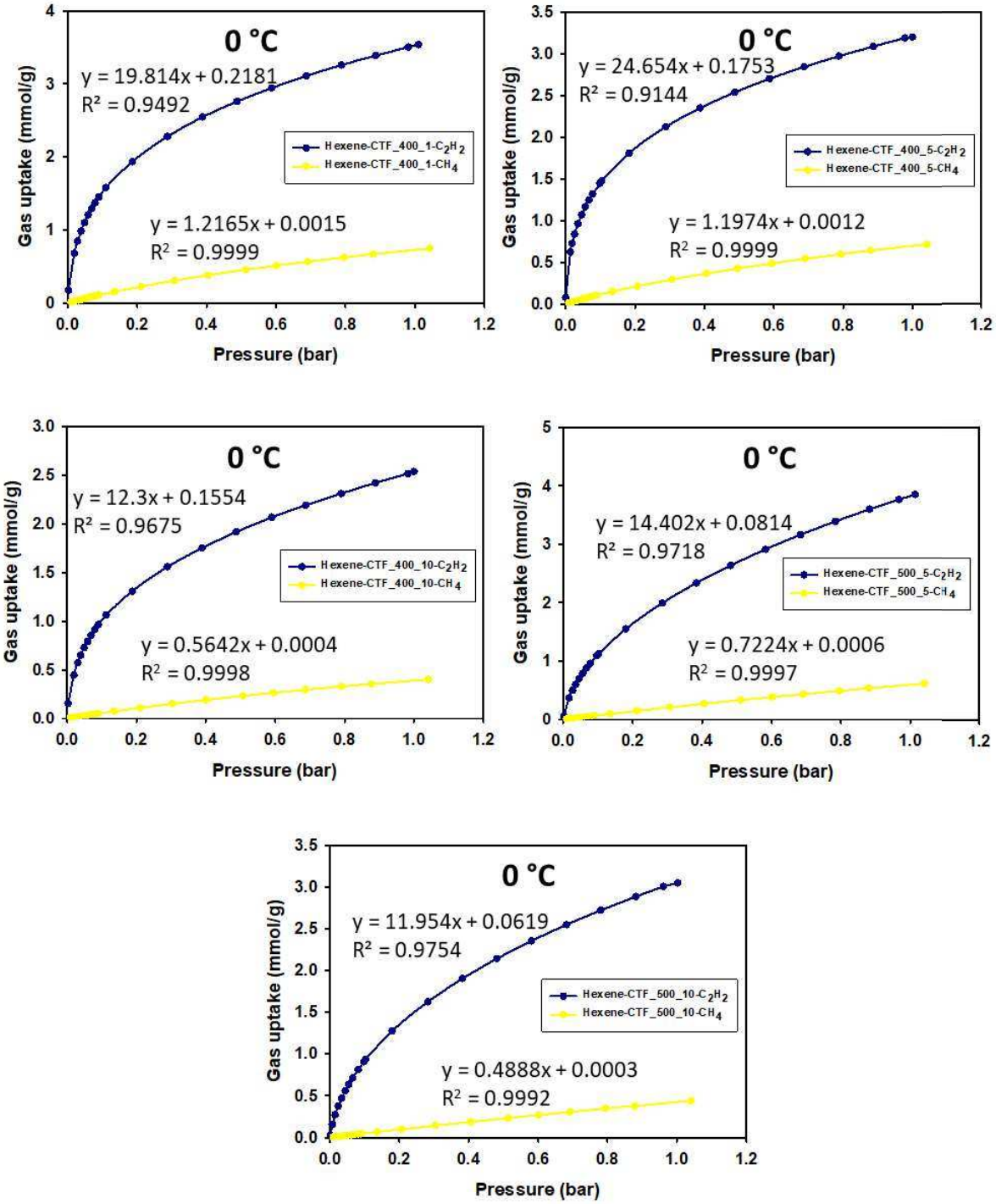

Figure S7: C_2H_2/CH_4 selectivity estimated using the ratio of the initial slopes in the Henry regime of the adsorption isotherms at 0°C.

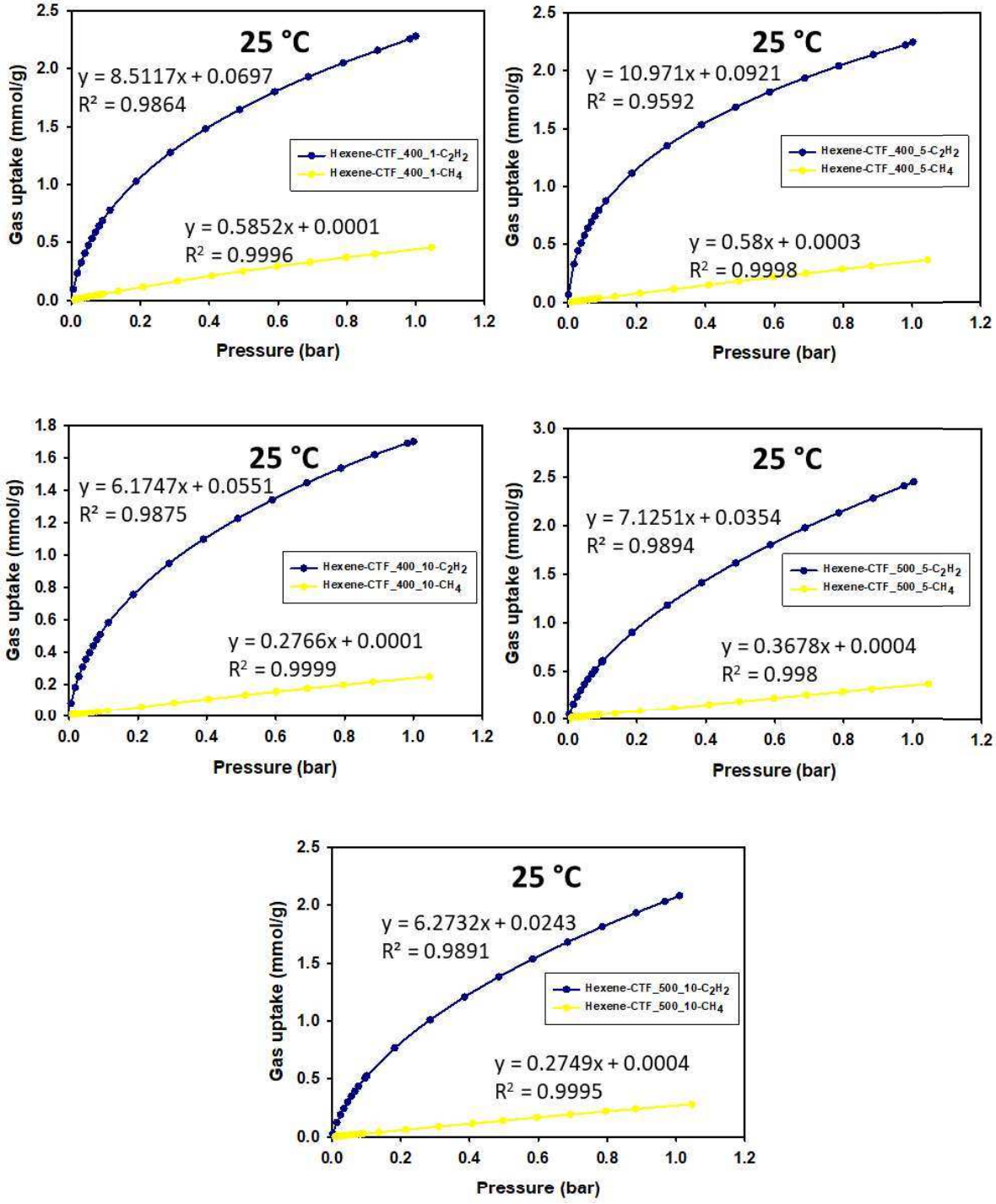

Figure S8: C_2H_2/CH_4 selectivity estimated using the ratio of the initial slopes in the Henry regime of the adsorption isotherms at 25°C.

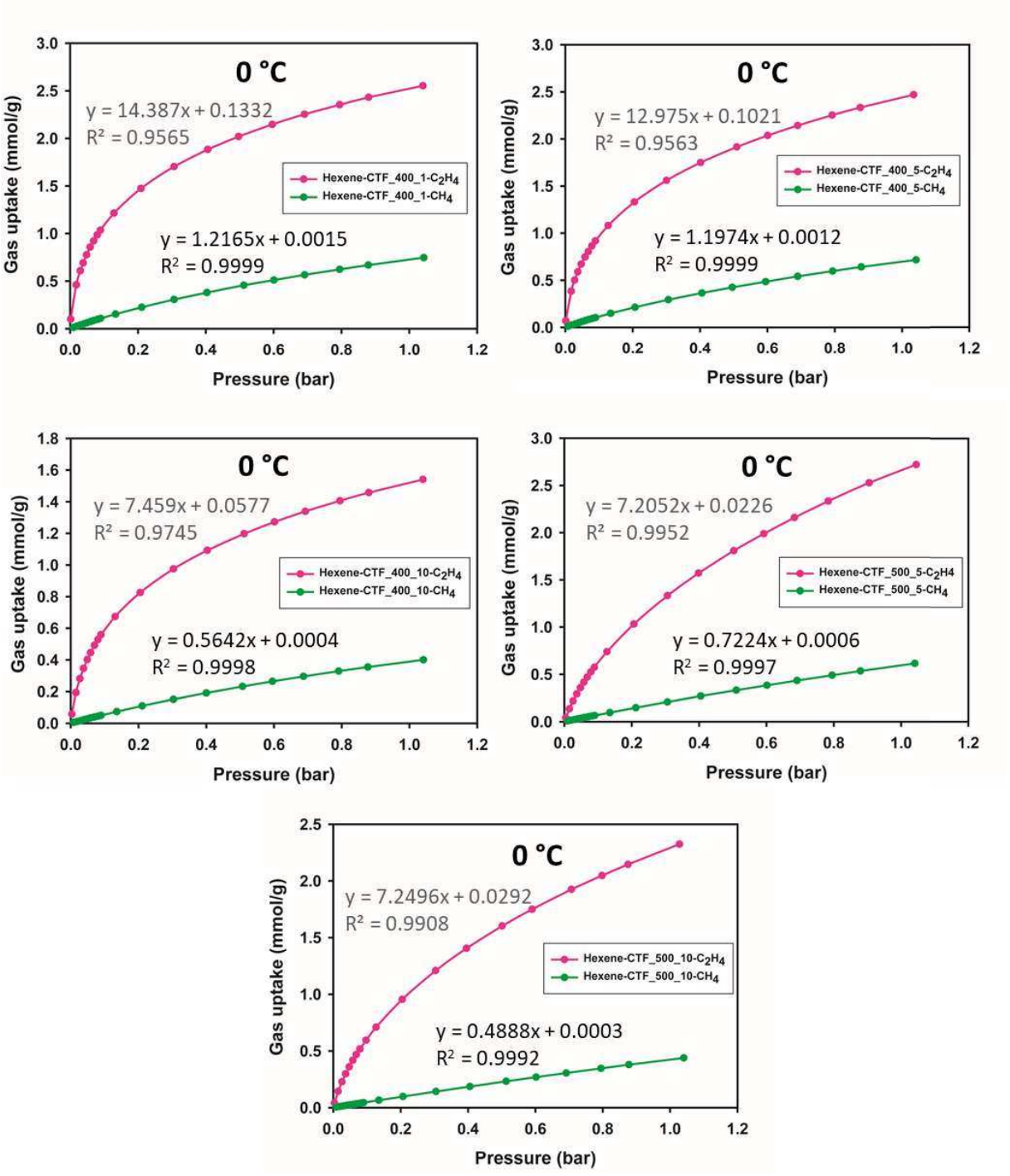

Figure S9: C_2H_4/CH_4 selectivity estimated using the ratio of the initial slopes in the Henry regime of the adsorption isotherms at 0°C.

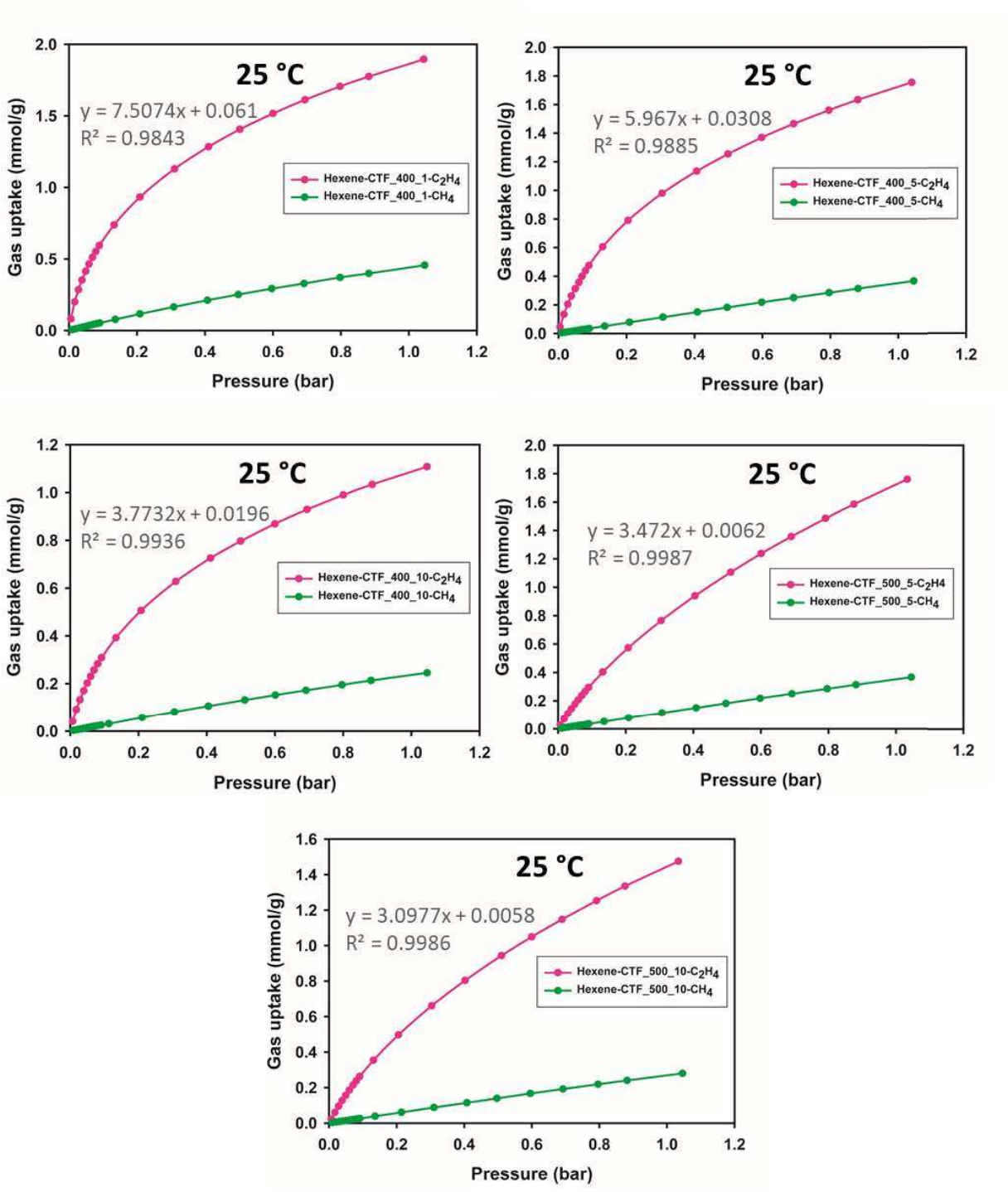

Figure S10: C_2H_4/CH_4 selectivity estimated using the ratio of the initial slopes in the Henry regime of the adsorption isotherms at 25°C.

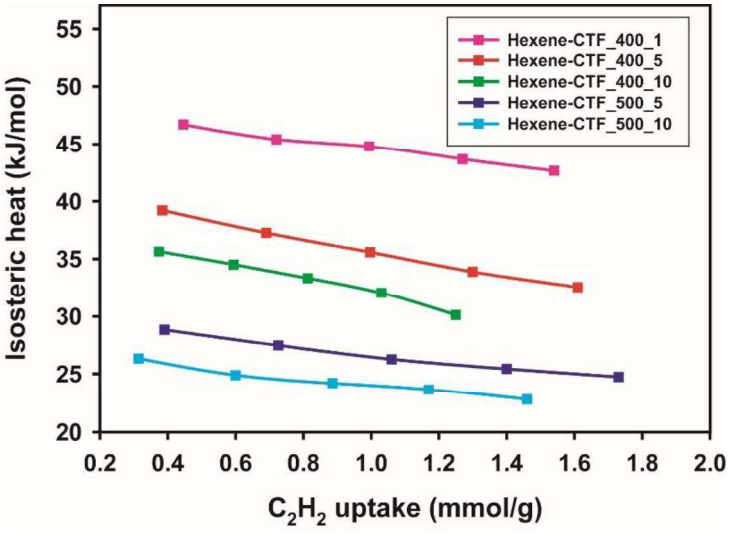

Figure S11: Isosteric heat of adsorption (Q_{st}) of C_2H_2 for all Hexene-CTFs.

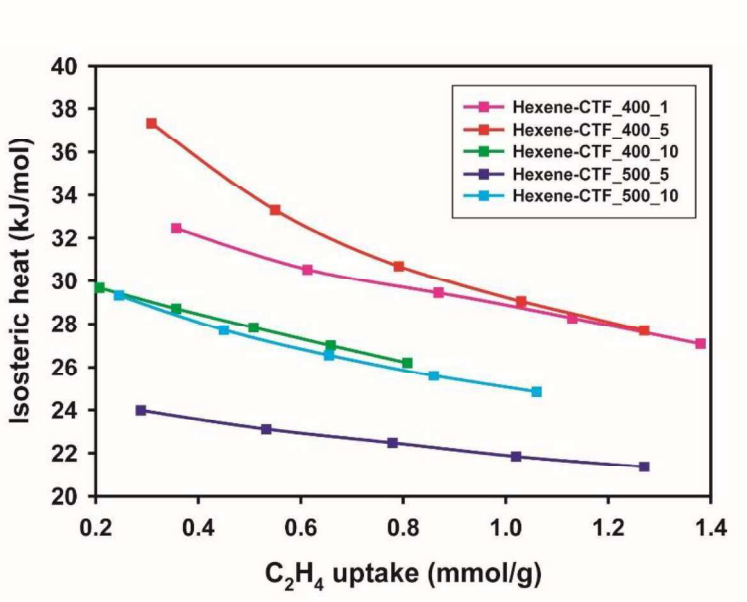

Figure S12: Isosteric heat of adsorption (Q_{st}) of C_2H_4 for all Hexene-CTFs.

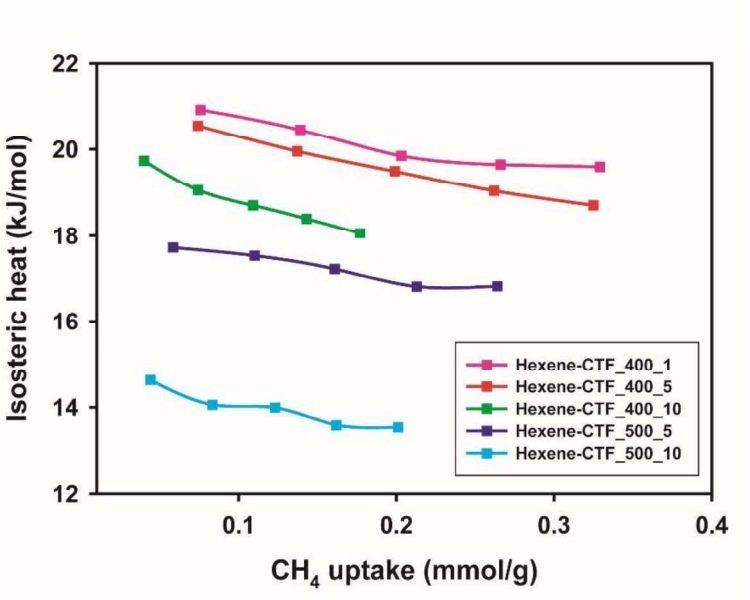

Figure S13: Isosteric heat of adsorption (Q_{st}) of CH_4 for all Hexene-CTFs.

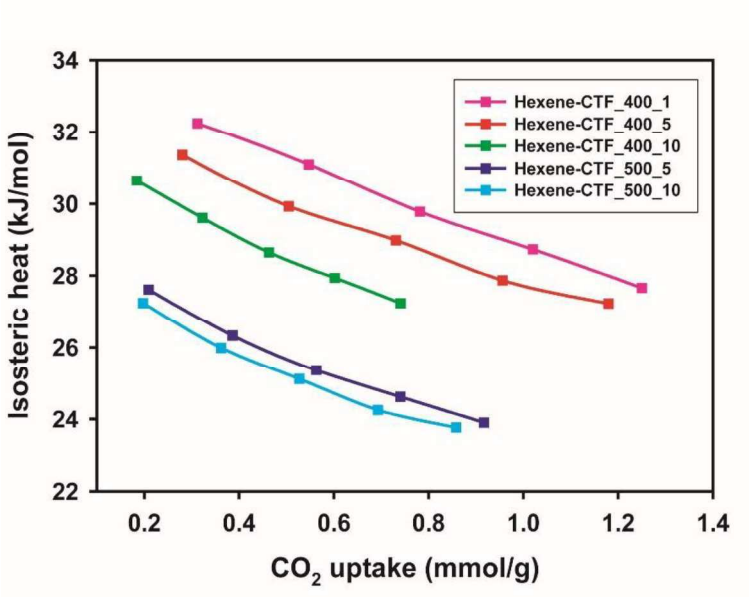

Figure S14: Isosteric heat of adsorption (Q_{st}) of CO_2 for all Hexene-CTFs.

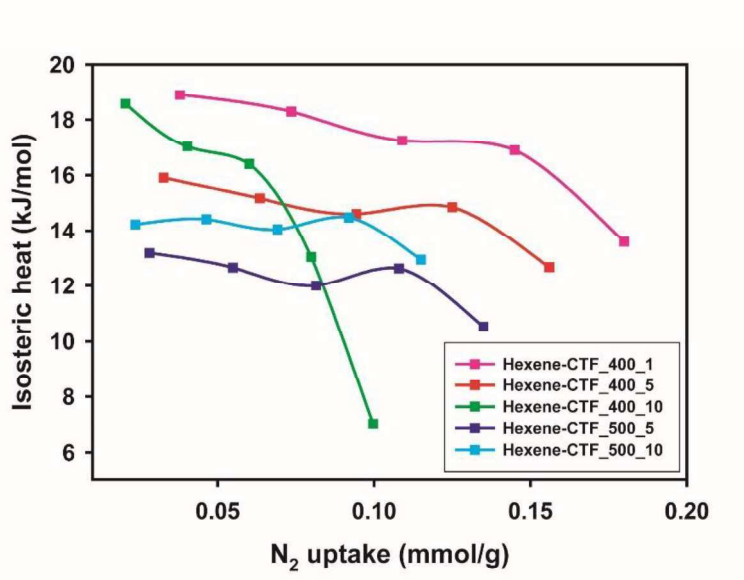

Figure S15: Isosteric heat of adsorption (Q_{st}) of N_2 for all Hexene-CTFs.

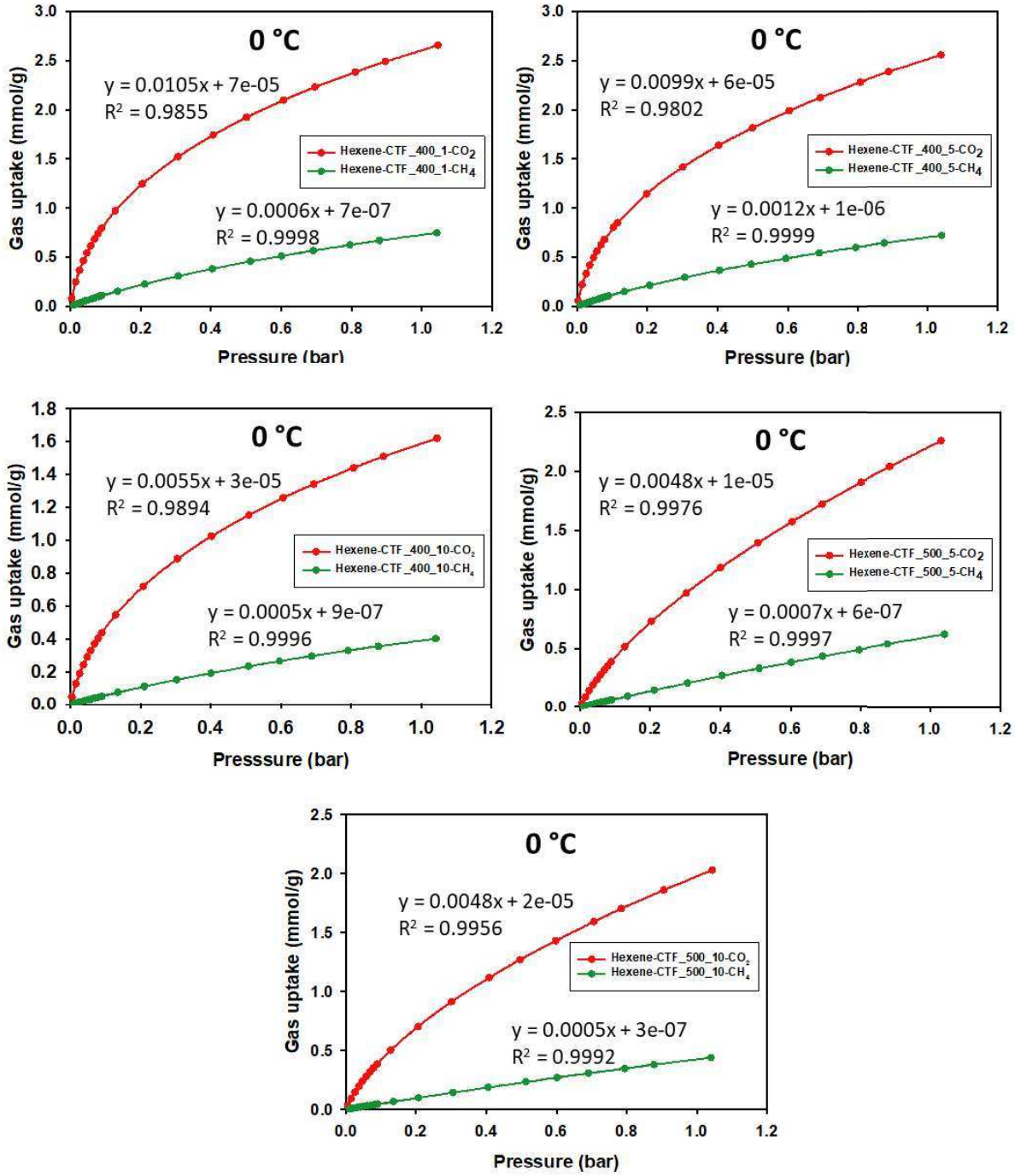

Figure S16: CO_2/CH_4 selectivity estimated using the ratio of the initial slopes in the Henry regime of the adsorption isotherms at 0°C.

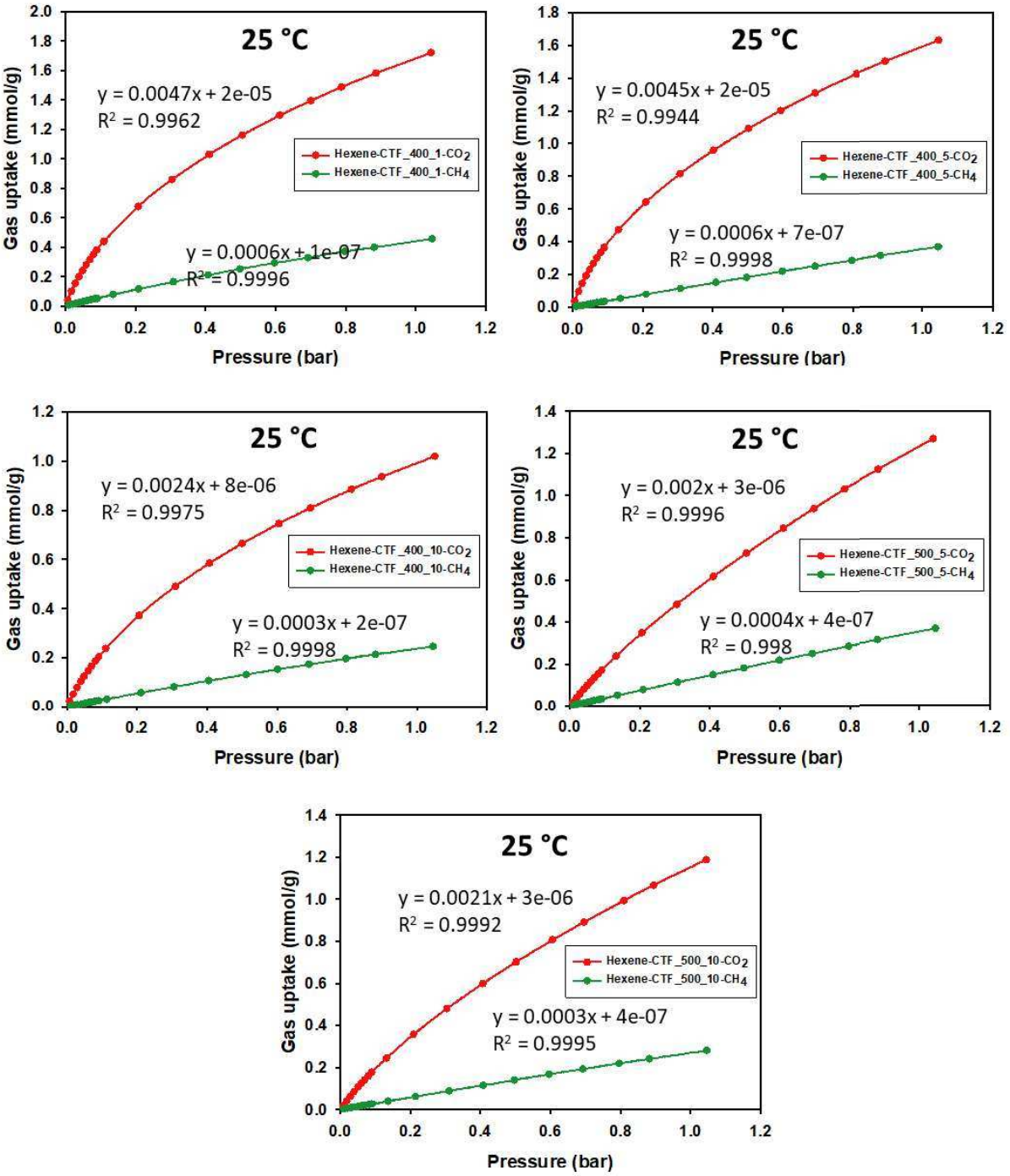

Figure S17: CO_2/CH_4 selectivity estimated using the ratio of the initial slopes in the Henry regime of the adsorption isotherms at 25°C.

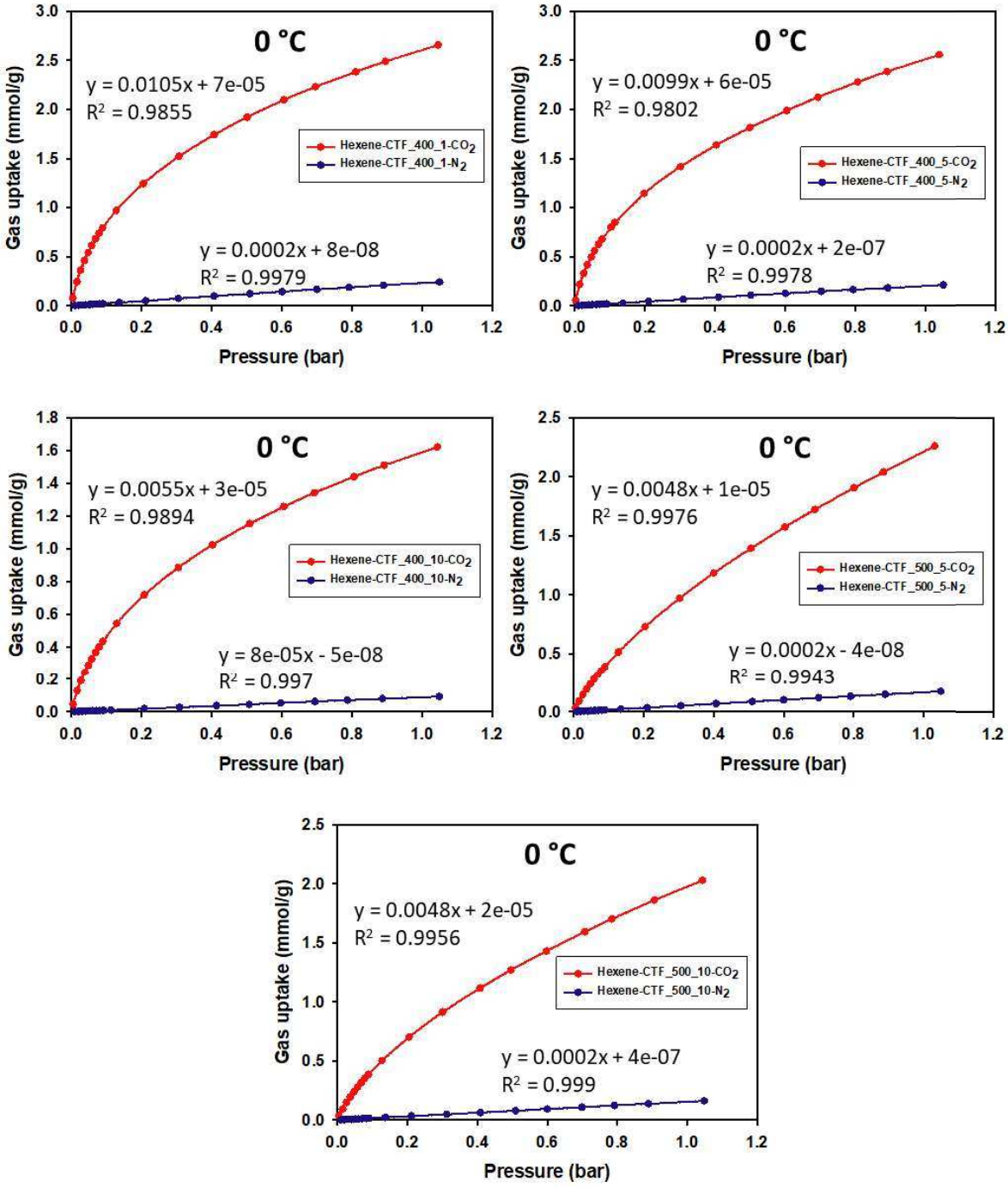

Figure S18: CO_2/N_2 selectivity estimated using the ratio of the initial slopes in the Henry regime of the adsorption isotherms at 0°C.

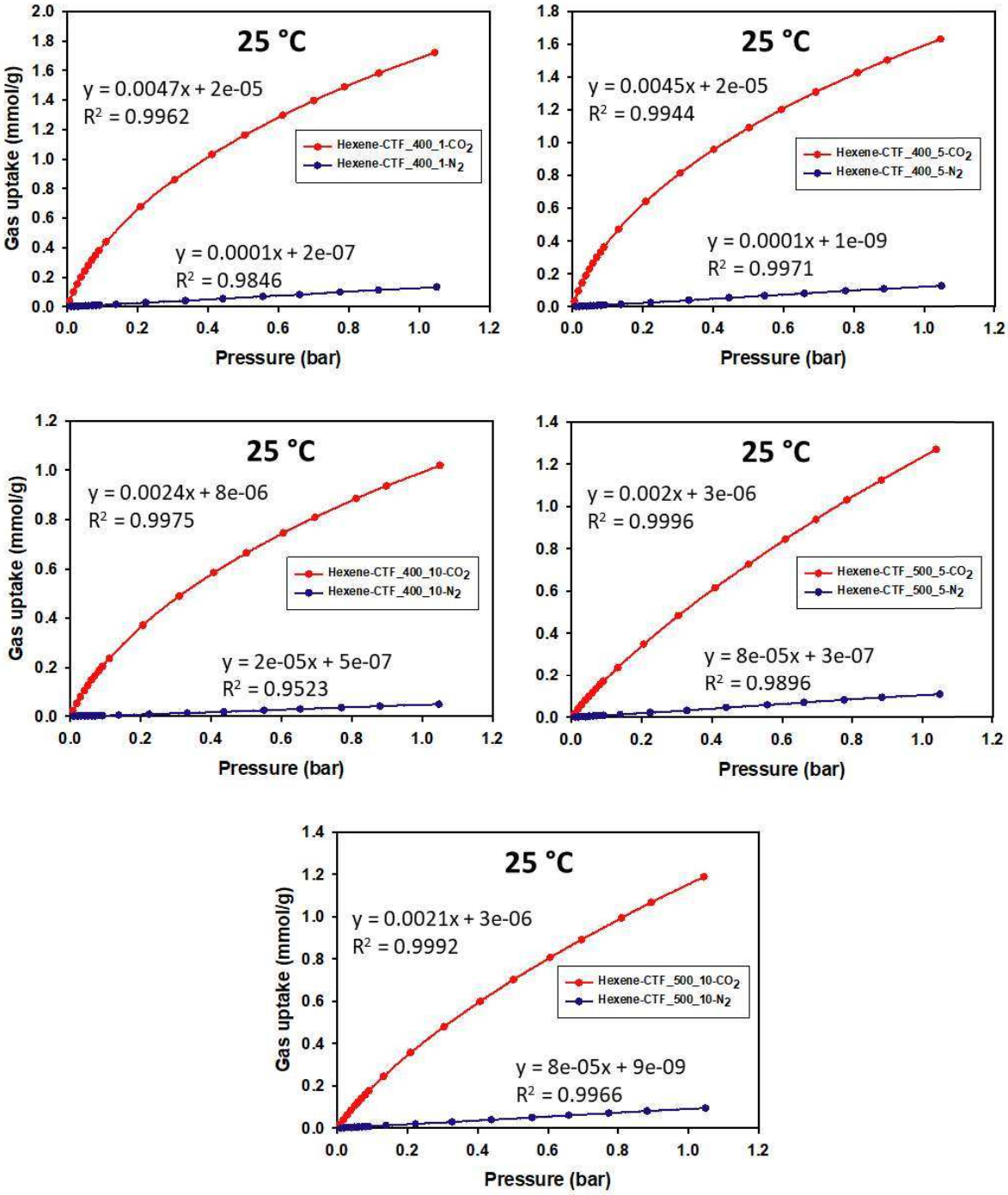

Figure S19: CO_2/N_2 selectivity estimated using the ratio of the initial slopes in the Henry regime of the adsorption isotherms at 25°C.